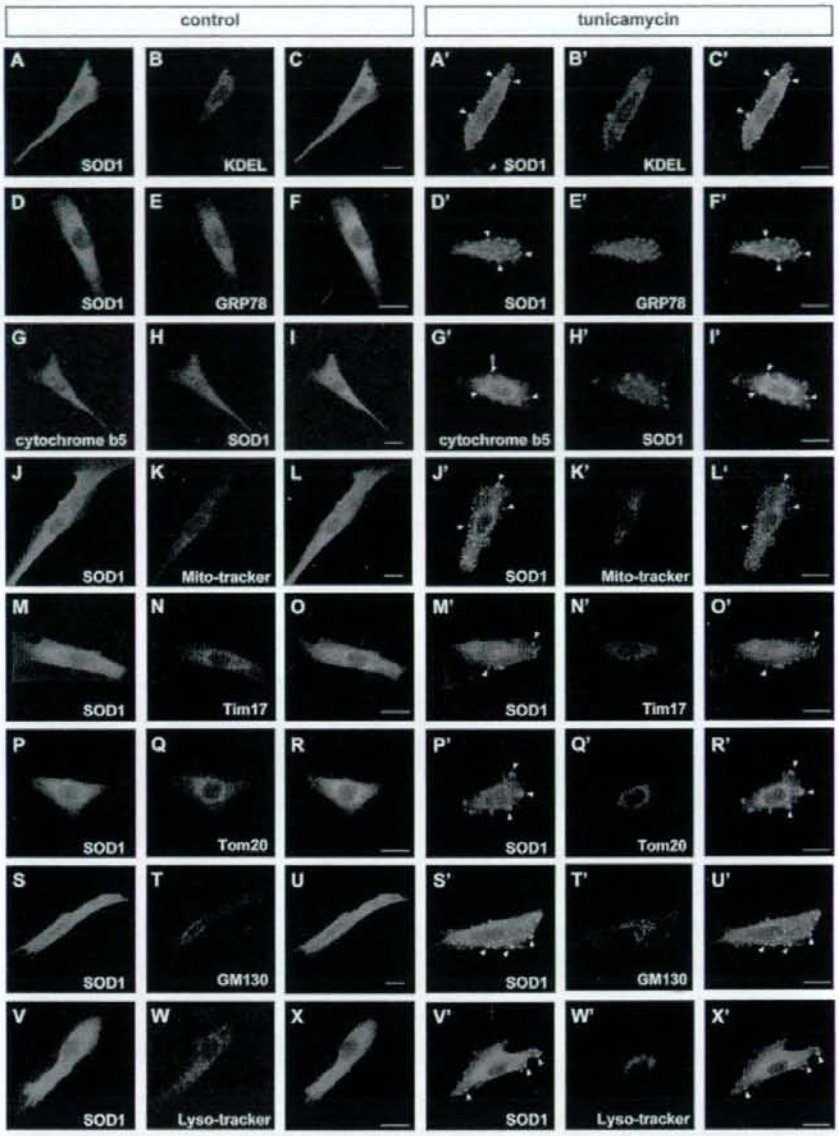

Figure 3. Positive translocation of SOD1 aggregates to ER, but not to the mitochondria, Golgi apparatus, or lysosomes. (**A–I, A'–I'**) Stress-dependent localization of SOD1 to the ER. L84V SOD1-expressing SK-N-SH cells were incubated for 24 h without (**A–I**) or with 1 μg/ml of tunicamycin (**A'–I'**). Then the cells were fixed and stained using an anti-SOD1 antibody (green; **A, D, A', D'**) and an anti-KDEL antibody (red; **B, B'**) or an anti-GRP78/BiP antibody (red; **E, E'**). GFP-cytochrome b5 were transfected to the cells and stained with anti-GFP (green; **G, G'**) and anti-SOD1 (red; **H, H'**) antibodies. Merged images (**C, F, I, C' F', I'**). The aggregates of SOD1 (arrowheads) are positive for KDEL, GRP78/BiP and cytochrome b5. (**J–R, J'–R'**) Analysis of SOD1 localization to the mitochondria. L84V SOD1-expressing SK-N-SH cells were treated as described in above. The locations of the mitochondria and SOD1 were visualized in L84V SOD1-expressing SK-N-SH cells using 100 nM Mito-tracker (red; **K, K'**), an anti-Tim17 antibody (red; N, N') or an anti-Tom20 antibody (red; **Q, Q'**) and an anti-SOD1 antibody (green; **J, M, P, J', M', P'**). Merged images (**L, O, R, L', O', R'**). (**S–U, S'–U'**) Investigation of SOD1 localization to the Golgi apparatus. L84V SOD1-expressing SK-N-SH cells were treated as described in above. Then the cells were stained with anti-SOD1 antibody (green; **S, S'**) and anti-GM130 antibody (red; **T, T'**). Merged images (**U, U'**). (**V-X, V'-X'**) Analysis of the localization of SOD1 to the lysosomes. A GFP-tagged L84V SOD1 vector was transfected into L84V SOD1-expressing SK-N-SH cells. After 24 h of incubation with 1 μg/ml of tunicamycin, the cells were incubated for a further 30 min with 100 nM Lyso-tracker (red; **W, W'**) to visualize the lysosomes. GFP channel (**V, V'**) Merged images (**X, X'**). Scale bars = 20 μm. Arrowheads indicate aggregated SOD1.
doi:10.1371/journal.pone.0001030.g003

(KDEL) containing protein and GRP78/BiP, suggesting SOD1 localization in ER (Fig. 3A–F, A′–F′). In order to confirm the SOD1 colocalization with ER, we utilized GFP conjugated cytochrome b5, a typical C-terminal anchored ER membrane protein. As expected, SOD1 showed the positive staining with cytochrome b5, indicating mutant SOD1 localization to ER (Fig. 3G–I, G′–I′). In the absence of stress, ER was located to the perinuclear region. However, treatment with tunicamycin seemed to cause its relocation to an abnormal region near the cell periphery. The aberrant distribution of ER following tunicamycin treatment was not observed in cells expressing wild type SOD1 (Fig. S1C′, F′ and I′). These results suggest deterioration of ER function and localization due to aggregation of mutant SOD1.

In light of previous reports identifying mutant SOD1 colocalization to the mitochondria [34,35,37], we also examined the potential colocalization of mutant SOD1 with mitochondria. In contrast to the results with markers for ER, the SOD1 aggregates induced by tunicamycin did not colocalize with the mitochondria marker Mitotracker, with Tim17 which marks the mitochondrial inner membrane nor Tom20 which marks the mitochondrial outer membrane (Fig. 3J′–R′). The localization of these SOD1 aggregates also did not correspond with the Golgi apparatus or the lysosomes, which were stained by anti-GM130 antibody and Lyso-tracker, respectively (Fig. 3S′–X′).

Our previous results in figure 3C′, F′ and I′ revealed aberrant redistribution of ER membranes in tunicamycin-treated mutant SOD1 expressing cells to the cell periphery region. To directly visualize the localization of ER, we performed electron microscopic analysis of tunicamycin-stressed cells expressing mutant SOD1. Figure 4A and B showed abnormal aggregates of rough ER, sac-like structures with surface ribosomes, associated with numerous free ribosomes. Mutant SOD1 localization to these peripheral aggregates was confirmed by immunoelectron microscopy (Fig. 4C), implying defective functional activities of ER and free ribosomes in cells expressing mutant SOD1.

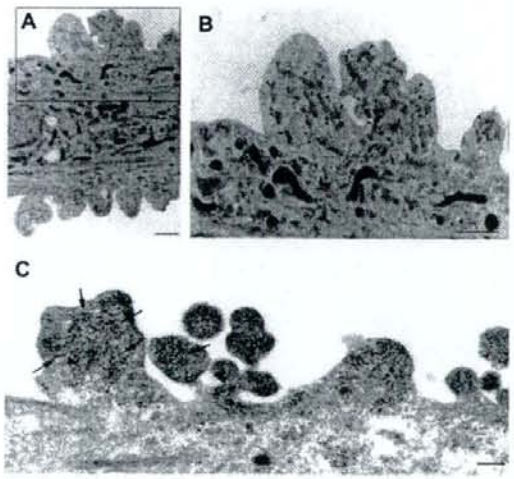

Figure 4. ER and SOD1 co-localization in peri-cytoplasmic membrane region. (**A**) Electron micrograph of L84V SOD1-expressing SK-N-SH cells after treatment with 1 μg/ml of tunicamycin for 24 h as described in Materials and Methods. (**B**) Enlargement of part of (**A**). Arrowheads indicate abnormal ER aggregates, where mutant SOD1 is localized as in Fig. 3C′ and 3E′. Scale bar = 1 μm. (**C**) SOD1 localization in peri-cytoplasmic membrane region. Cells were treated as described in (**A**) and immune electron micrograph was obtained as described in Materials and Methods. Arrows show SOD1 immunoreactive in ER.
doi:10.1371/journal.pone.0001030.g004

LBHI/Ast-HI-like Inclusions are induced by ER stress.

Wate et al. [28] reported that neuronal LBHI in G93A SOD1 transgenic mice are immune reactive for GRP78/BiP, an ER resident component of the UPR response. As shown in figures 3A′-I′ and 4C, mutant SOD1 localized to the ER following stress induction by tunicamycin. These SOD1 aggregates shared additional features with LBHI/Ast-HI, namely eosin positivity and ubiquitin immune reactivity. Those observations led us to consider whether ER stress would eventually induce the formation of full-fledged LBHI/Ast-HI. To test this hypothesis, we examined whether inclusion bodies containing mutant SOD1 developed in L84V SOD1-expressing cells subjected to ER stress. Consistent with this idea, eosinophilic hyaline inclusions (~10 to 20 μm in diameter) with a pale core, which are similar to neuronal LBHI/Ast-HI in the spinal cord of ALS patients harboring a SOD1 mutation, developed within 24 hrs of exposure to tunicamycin (Fig. 5A), but not in cells expressing wild type SOD1 (data not shown). In fact, the eosin-positive LBHI/Ast-HI-like hyaline inclusions (LHIs) were morphologically similar to the Ast-HI seen in the spinal cord of transgenic L84V SOD1 mice at the symptomatic stage (Fig. 5A and D). Furthermore, ultrastructual analysis revealed that the LHIs in neuroblastoma cells were composed of granule-coated fibrils (approximately 15–25 nm in diameter) and granular materials, which are the typical morpho-

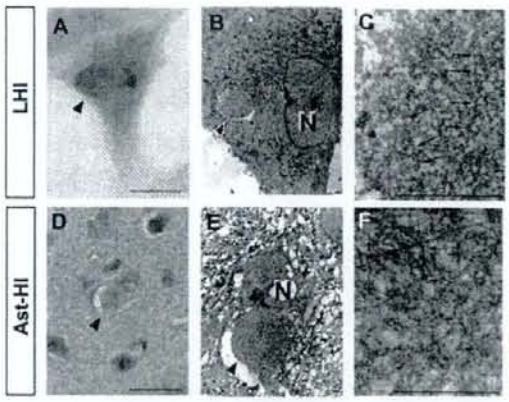

Figure 5. LHIs containing granule-coated fibrils are morphologically identical with Ast-HI from L84V transgenic mice. (**A–F**) Comparison of a LHI induced by ER stress in an L84V SOD1-expressing SK-N-SH cell (A–C) and Ast-HI in the spinal cord of a transgenic L84V SOD1 mouse (D–F). (**A**) An eosinophilic LHI in the cytoplasm of the SK-N-SH cell expressing L84V SOD1 cell was induced by treatment with 1 μg/ml of tunicamycin for 24 h (scale bar = 20 μm). (**B**) Electron micrograph of a hyaline inclusion (arrow) obtained by the direct epoxy resin-embedding method after decolorization of the HE-stained section shown in (**A**). N, nucleus; ×3000 (scale bar = 1 μm). (**C**) At a high magnification, the inclusion is composed of granule-coated fibrils (arrows) approximately 15–25 nm in diameter and granular materials. ×16000 (scale bar = 1 μm). (**D**) An eosinophilic Ast-HI from a transgenic L84V SOD1 mouse. (**E**) Electron micrograph of an Ast-HI obtained by the direct epoxy resin-embedding method mentioned in (**B**). N, nucleus; ×2000 (scale bar = 1 μm). (**F**) Enlargement of (**E**). ×16000 (scale bar = 1 μm). Note that the fibrils observed in (**C**) and (**F**) are ultrastructually identical.
doi:10.1371/journal.pone.0001030.g005

logical hallmarks of mutant SOD1-linked FALS, and were identical with the Ast-HI found in L84V SOD1 mice (Fig. 5C, F; [38]). These results suggest that LBHI/Ast-HI in FALS patients might be provoked by ER stress as we observed for LHIs.

We further explored the molecular similarity between the LHI and LBHI/Ast-HI, using double-label immunocytochemistry. As shown in figure 6A–D, LHIs induced by tunicamycin are immunopositive for anti-SOD1 and anti-ubiquitin antibodies, consistent with the LBHI/Ast-HI features. In the spinal cord of G93A SOD1 mutant mice at the symptomatic stage, neuronal LBHI show GRP78/BiP immunoreactive, suggesting the involvement of ER resident protein [28]. Therefore, we examined whether LHIs also contain ER resident protein. As expected, LHI showed anti-KDEL positivity, indicating the involvement of ER resident proteins such as calreticulin, GRP 94, PDI and GRP78/BiP in LHI development (Fig. 6E and F). Furthermore, Ast-HI in spinal cord of L84V SOD1 transgenic mice at symptomatic stage also showed KDEL positive (Fig. 6G and H), meaning that the principle features of these inclusions in neuroblastoma cells and the LBHI/Ast-HI of FALS patients are the same and implying LHI and LBHI/Ast-HI might develop in similar procedure.

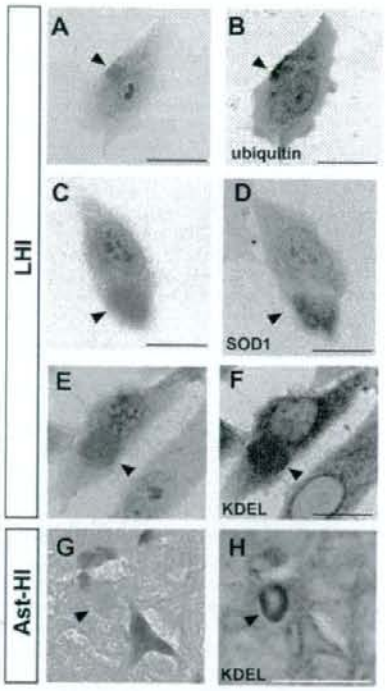

Figure 6. Positive immunoreactive against ubiquitin, SOD1 and KDEL of LHIs. (**A–D**) LHIs show immunoreactive against ubiquitin and SOD1. Eosinophilic LHIs in SK-N-SH cells (arrowheads in **A** and **C**) induced by tunicamycin were immunostained for ubiquitin (**B**) and SOD1 (**D**) after de-colorization. (**E–H**) KDEL immunoreactive in both LHI and Ast-HI. Eosinophilic LHI in SK-N-SH cells (arrowhead in **E**) and Ast-HI in spinal cord of L84V SOD1 mouse (arrowhead in **G**) were immunostained against anti-KDEL antibody after de-colorization (**F, H**). Scale bar = 20 μm

doi:10.1371/journal.pone.0001030.g006

Abnormal ER aggregated around peri-nuclear region with numerous free ribosomes at presymptomatic stage of Ast-HI in L84V SOD1 mice.

To further explore the relationship of LHI to the development of LBHI/Ast-HI in FALS patients with mutant SOD1, we performed ultrastructual examination of transgenic L84V SOD1 mice, which show neuronal LBHI and Ast-HI at symptomatic stage (Fig. 5D–F, 6G–H; [35]). We examined the mice at the presymptomatic stage in the hope of detecting precursors to hyaline inclusion bodies. In spinal cord neurons of the pre-symptomatic L84V SOD1 transgenic mice, we observed aberrant aggregation of electron-dense rough ER around the peri-nuclear region with numerous free ribosomes, which were suspected to be producing mutant SOD1 (Fig. 7). This suggests that the aberrant SOD1 fibrils observed in spinal neurons of these mice at later

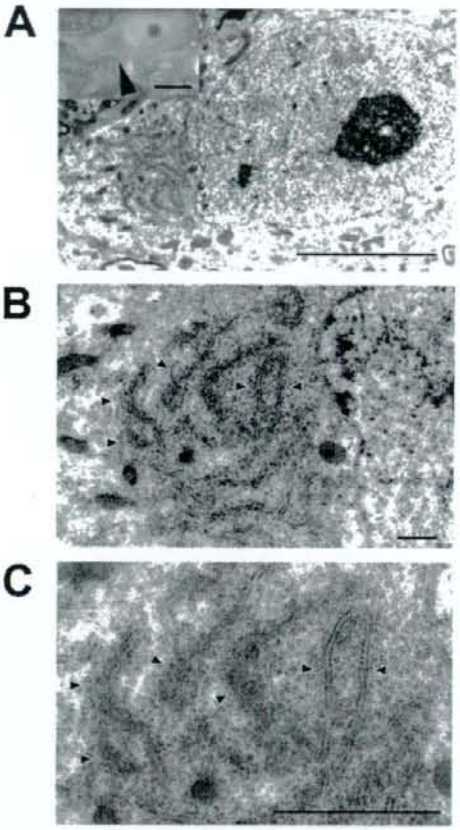

Figure 7. ER shows abnormal aggregation with numerous free ribosomes in L84V SOD1 mouse at presymptomatic stage. (**A–C**) Electron micrographs of a neuron obtained from an L84V SOD1 transgenic mouse containing ER aggregates. The inset in (**A**) shows a cytoplasmic inclusion-like structure (arrowhead) stained with toluidine blue. (**A**) ×3500 (scale bars = 20 μm). (**B**) ×8000 (scale bar = 1 μm). (**C**) ×15000 (scale bar = 1 μm). Arrowheads indicate abnormal ER aggregates.

doi:10.1371/journal.pone.0001030.g007

stages might be produced by cooperative activity of ER and ribosomes. These inclusion-like structures with abnormal accumulation of ER seemed likely to represent a precursor to the later neuronal LBHI observed in this line. These results imply that the deterioration of ER function and the involvement of ER might be important for formation and developing neuronal LBHI/Ast-HI in mutant SOD1 harboring FALS patients.

DISCUSSION

Aggregated proteins or inclusions are a pathological hallmark and possible causative agent of several neurodegenerative disorders including ALS [39]. While LBHI/Ast-HI have been established as morphological hallmarks of mutant SOD1-linked FALS, little is known about the formation of these structures in neurons [6]. Several in vitro systems have been provided for analysis mutant SOD1 aggregation [35,36,40], however, the relationship between mutant SOD1 aggregation *in vitro* and pathological hyaline inclusions *in vivo* remains unclear. The LHI we observed in SK-N-SH cells expressing mutant SOD1 provide a direct link between *in vitro* and *in vivo* SOD1 aggregation. To our knowledge, this is the first study to show reproducible induction of LBHI/Ast-HI like structures meeting the criteria of inclusion bodies [24,26,31,38,41].

LBHIs/Ast-HIs in human FALS consist of a chaotic mixture of cytoplasmic proteins (such as SOD1, copper chaperone for SOD (CCS), peroxiredoxin 2, and glutathione peroxidase 1), cytoskeletal proteins (such as tubulin, tau protein, and phosphorylated- and nonphosphorylated neurofilament), nuclear proteins (such as neuron-specific enolase) and synaptic proteins (such as synaptophysin [24,38,41–43]). Recently, it has been published that GRP78/BiP, an ER resident chaperon protein, is also co-localized with LBHI of G93A SOD1 mice [28]. GRP78/BiP is molecular chaperone protein induced by IRE1 in response to aberrant protein folding and promotes proper protein folding. In this context, GRP78/BiP may be acting as part of the UPR response to resolve granule coated fibrils. Tobisawa et al. [35] reported increased protein levels of GRP78/BiP in motor neurons of mutant SOD1 transgenic mice, suggesting that the motor neurons in their model suffer from 'ER stress'. While the importance of ER stress or proteosome malfunction in formation of mutant SOD1 aggregates has been established [35,36,40], the mechanisms by which mutant SOD1 forms LBHI/Ast-HI in FALS remain poorly understood. In this study, we present three lines of evidence for the involvement of ER stress in early events in LBHI/Ast-HI formation. First, ER stress in neuroblastoma cells expressing mutant SOD1 results in SOD1- and ubiquitin-immunopositive LHIs, compatible with LBHI/Ast-HI, composed of granule-coated fibrils approximately 15–25 nm in diameter and granular materials (Figs. 5 and 6). Secondly, we observed similar structures in the spinal cord of L84V SOD1 transgenic mice at pre-symptomatic stages, including abnormal electron dense, i.e. stressed, ER and numerous free ribosomes. (Figs. 4 and 7). Third, positive staining against anti-KDEL antibody, which recognizes ER resident proteins such as calreticulin, GRP 94, PDI and GRP78/BiP, were observed in both the LHI and Ast-HI of L84V SOD1 transgenic mice at symptomatic stages (Fig. 6E–H). These findings support the hypothesis that ER stress induces LBHIs/Ast-HIs creation in FALS patients with mutant SOD1. Taken together, these observations suggest that LHI in neuroblastoma cells and LBHI/Ast-HI in FALS patients might develop through similar processes.

In this study, we presented evidences that ER stress causes aggregates of mutant SOD1 and formation of LHI which is compatible with LBHI/Ast-HI. However, other questions arise from these results. 1) Why did same stress induce the different outcome of mutant SOD1 aggregation in the neuroblastoma? 2) Are the smaller aggregates competent to develop to LHIs? To answer these questions, we sought without success to identify the origin of the granule coated fibrils or SOD1 containing filamentous structure (e.g. less densely coated fibrils) in the smaller SOD1 aggregates localized to ER in L84V SOD1 expressing cells. Nevertheless, we found common features between the small aggregates in L84V SOD1 expressing SK-N-SH cells and neuronal LBHI-precursor in L84V transgenic mice, including regions of abnormal ER aggregation surrounded by abundant free ribosomes (Fig. 4B and Fig 7C). Furthermore, LHI and Ast-HI were immunopositive for the KDEL peptide present in ER-resident proteins, suggesting the involvement of ER itself in formation or development of LBHI/Ast-HI (Fig. 6E–H). We suggest that aberrant SOD1 fibril might be produced by cooperative activity of ER and ribosomes. To answer the questions, careful observation of LHI with time lapse analysis is needed.

It remains unclear why the major symptoms of ALS in patients with mutant SOD1-linked FALS do not develop until middle age, but we speculate that age-dependent changes in responses to ER stress might provide an answer. Under normal conditions, newly synthesized and misfolded proteins are refolded by chaperons such as GRP78, 94, calnexin, and calreticulin. This UPR response may be more robust in younger FALS patients and might be the reason the proteins aggregates are not observed in young patients even though mutant SOD1 is expressed. However, a decrease in protein folding or chaperone capability may occur with aging, and accumulation of misfolded proteins in the ER lumen may gradually lead to ER stress [44]. Consistent with this idea, Tobisawa et al. reported mutant SOD1 retention in the ER in COS7 cells [35] and Kikuchi et al. reported age-dependent increase of mutant SOD1 aggregation to ER in spinal cord of G93A SOD1 mice, suggesting ER dysfunction might be caused by mutant SOD1 [36]. Prolonged ER stress associated with insufficient degradation of misfolded proteins would subsequently activate apoptotic pathways. Nakagawa et al. reported that caspase-12, the ER resident caspase, is specifically cleaved and activated by ER stress, and that cells derived from mice lacking caspase-12 are resistant to ER stress [16]. In the spinal cords of G93A SOD1 mice, caspase-12 is activated in symptomatic period and can be inhibited by overexpression of XIAP (X-linked inhibitor of apoptosis protein [45,46]. Then, we analyzed activation of caspase-4 (the human orthologue of rodent caspase-12) following tunicamycin treatment. As expected, the SOD1 aggregates of the L84V SOD1-expressing neuroblastoma cells colocalized with caspase-4 (unpublished data), implying caspase-4 might contribute to cell death in our model system.

Although it can take longer than 30 years for LBHI/Ast-HI to develop in FALS patients, we could induce the formation of morphologically similar LHI within 24 hours in our simple model. Detection of the molecular targets for ER stress-induced hyaline inclusions of mutant SOD1 in our model might lead to the development of therapy that can prevent the progression of mutant SOD1-linked FALS. Ultimately, our study should contribute to the development of a simple system to analyze novel therapies for ALS.

MATERIALS AND METHODS

Transgenic Mice

Transgenic mice for mutant human SOD1^{L84V} (C587BL/6 background) were created (M. Kato, et al. Transgenic mice with ALS-linked SOD1 mutant L84V. Abstract of the 31st Annual Meeting of Society for Neuroscience, San Diego, 2001). Mice were genotyped by PCR to detect the mutant SOD1 transgene using

the following primers: forward, TTGGGAGGAGGTAGTGATTA; reverse, GCTAGCAGGATAACAGATGA. The onset of symptoms was at 5–6 months and the initial sign of the disease was usually weakness in their hindlimbs, while approximately 10% of the mice first showed weakness in their forelimbs.

Chemicals and antibodies

We used the following antibodies: anti-SOD1 polyclonal antibody (pAb; Chemicon, Temecula, CA); anti-ubiquitin pAb and anti-KDEL mAb (Stressgen, Victoria, BC. Canada); anti-Tim17 pAb and anti-Tom20 pAb (grateful gifts by Dr. Otera and Prof. Mihara [47,48]); Alexa Fluor 488-conjugated anti-sheep IgG, Alexa Fluor 588-conjugated anti-mouse IgG antibody, and Alexa Fluor 588-conjugated anti-rabbit IgG antibody (Molecular Probes, Eugene OR); biotinylated anti-sheep IgG (Vector Laboratories, Burlingame, CA); anti-FLAG mAb (Sigma, woodlands, USA); anti-myc pAb and anti-GFP-mAb (Santa Cruz, Santa Cruz, CA); HRP-conjugated anti-sheep IgG (Jackson ImmunoResearch Laboratories Inc., West Grove, PA); and HRP-conjugated anti-mouse IgG and HRP-conjugated anti-rabbit IgG antibody (Cell Signaling Technology, Beverly, MA). Tunicamycin was obtained from Sigma.

Cell culture and induction of ER stress

SK-N-SH human neuroblastoma cells were obtained from the Riken Cell Bank (Tsukuba, Japan), and were cultured in α-MEM (Invitrogen) containing 10% fetal bovine serum at 37°C under 5% CO_2. These cells were transfected with pcDNA3.1-hSOD1 and pcDNA3.1-hL84V-SOD1 to cause overexpression of wild-type or L84V mutant SOD1, respectively. G418 resistant stable neuroblastoma cell lines expressing equal levels of endogenous and exogenous SOD1 were established. In all experiments, we used cultures that were at 70–80% confluence to avoid the influence of stress induced by overgrowth. On the day of stimulation, fresh medium was added more than 1 h before exposure to stress in order to ensure the same conditions for each culture.

Western blot analysis

SK-N-SH cells stably expressing wild-type or L84V SOD1 were washed with PBS, harvested, and lysed in TNE buffer containing 1 mM PMSF and 1% SDS. 10 μg of protein was subjected to 12% SDS-PAGE and transferred to a PVDF membrane (Millipore Corp.). The membrane was blocked with 5% skim milk and incubated with anti-SOD1 antibody (1:1500 dilution), followed by incubation with an HRP-conjugated secondary antibody. Proteins were visualized with an ECL detection system (Amersham-Pharmacia).

Immunocytochemistry

SK-N-SH cells stably expressing wild-type SOD1 or L84V SOD1 were treated with 1 μg/ml of tunicamycin for 24 h. Then the cells were fixed with Zamboni's solution (0.1 M phosphate-buffered saline (PBS; pH 7.4) containing 2% paraformaldehyde (PFA) and 21% picric acid), rinsed in 0.1 M PBS, and incubated for 30 min in 0.3% H_2O_2 to eliminate endogenous peroxidases. Next, the cells were incubated overnight at 4°C with the primary antibody (a polyclonal sheep anti-SOD1 antibody; Calbiochem) at 1:1000 in 0.1 M PBS containing 0.3% Triton X-100 and 3% bovine serum albumin (BSA). After washing in 0.1 M PBS, cells were incubated for 30 min with the secondary antibody (biotinylated anti-sheep IgG) (Vector Laboratories). After amplification with avidin-biotin complex from the ABC kit (Vector Laboratories), reaction products were visualized with 0.05 M Tris-HCl buffer (TBS; pH 7.6) containing 0.02% diaminobenzidine tetrahydrochloride (DAB) and 0.01% hydrogen peroxide. Finally, the cells were counterstained with Mayer's hematoxylin and eosin (HE).

Co-immunoprecipitation assay utilizing ubiquitin

Lysates of pcDNA3.1-myc-tagged ubiquitin (a kind gift from Dr. Niwa and Prof. Sobue [32])-transfected SK-N-SH cells stably expressing wild-type SOD1 or L84V SOD1 were prepared using TNE buffer (10 mM Tris-HCl, (pH 7.4), 150 mM NaCl, and 1 mM EDTA) containing 1 mM phenylmethylsulphonyl fluoride (PMSF), 2 μg/ml aprotinin, and 1% Nonidet P-40 after treatment with or without 4 μg/ml ALLN for 12 h. Then, 1 μg of anti-FLAG antibody was added to 400 μg of lysate, followed by incubation at 4°C for at least 3 h. Protein G-Sepharose (10 μl gel) was then added and incubation was done with rotation at 4°C for 1 h. The immunoprecipitate was subjected to SDS-PAGE and transferred to a polyvinylidene fluoride (PVDF) membrane. The membrane was blocked with 5% skim milk and then was incubated with anti-Myc antibody (1:1000 dilution), followed by incubation with an HRP-conjugated secondary antibody. Proteins were visualized with an ECL detection system (Amersham-Pharmacia).

Immunofluorescence and chemifluorescence

SK-N-SH cells expressing wild-type SOD1 or L84V SOD1 were incubated with or without tunicamycin or ALLN, rinsed in 0.02 M PBS, and fixed in Zamboni's fixative. Then the cells were incubated overnight at 4°C with an anti-SOD1 antibody (1:1000 dilution) and either anti-KDEL (1:500 dilution), anti-GM130 (1:500 dilution) or anti-ubiquitin (1:500 dilution) antibody in 0.02 M PBS containing 0.3% Triton X-100 and 3% BSA. Next, the cells were treated with fluorescent dye (Alexa Fluor 488)-conjugated donkey anti-sheep IgG (SOD1; 1:1000 dilution), fluorescent dye (Alexa Fluor 568)-conjugated goat anti-mouse IgG (KDEL, GM130; 1:1000 dilution), and goat anti-rabbit IgG (ubiquitin; 1:1000) as the secondary antibodies for 1 h at RT in 0.02 M PBS containing 3% BSA. Examination was done under a Zeiss LSM 510 microscope. For detection of SOD1 colocalization with cytochrome b5, pCMV b5-EGFP vector was transfected to the cells (kind gift from Dr. Otera and Prof. Mihara; [49]). The GFP signal was enhanced by anti-GFP antibody staining (1:100). In order to determine the localization of SOD1 in living cells, SK-N-SH cells expressing wt and L84V SOD1 were transfected with a pcDNA3.1-GFP-tagged wt and L84V SOD1 plasmid, respectively. After treatment with tunicamycin for 24 hr, the cells were further incubated with Mito-tracker or Lyso-tracker (Molecular Probes) for 30 min to visualize the mitochondria or lysosomes, respectively. Then the cells were rinsed at least three times in 0.1 M PBS and fixed with Zamboni's solution for examination under a LSM 510 confocal microscope (Zeiss, Osaka, Japan).

Electron microscopy

SK-N-SH cells stably expressing L84V SOD1 were exposed to 1 μg/ml tunicamycin for 24 h and then fixed at room temperature (RT) for 1 h in 0.1 M phosphate buffer (PB) containing 2.5% glutaraldehyde (GA) and 2% paraformaldehyde. Subsequently, the cells were post-fixed in 1% OsO_4 at RT for 1 h, dehydrated in a graded ethanol series, and embedded in epoxy resin (Quetol 812; Nisshin EM Co.). Areas containing cells with aggregates were block-mounted in epoxy resin by the direct epoxy-resin embedding method and cut into 90-nm sections. The sections were counterstained with uranyl acetate and lead citrate, and then examined using an H-7100 electron microscope (Hitachi).

Immune Electron microscopy

As with immunocytocemistry methods above, after fixation with Zamboni solution containing 0.1% GA, the cells with anti-SOD1 antibody were developed with DAB. Then, they were post-fixed in 1% OsO4 in 0.1 M PB at RT for 30 min after 1% GA in 0.1M PB re-fixation. The samples were dehydrated in a graded ethanol series and then embedded in Quetol 812. Areas containing cells with aggregate morphology were block-mounted and cut into 90-nm sections. The sections were counterstained with uranyl acetate and lead citrate, and then examined with an H-7100 electron microscope.

Analysis of inclusion bodies (light microscopy and electron microscopy)

Sections of SK-N-SH cells containing eosinophilic hyaline inclusion bodies and spinal cord sections from transgenic SOD1 L84V mice were decolorized, rehydrated, rinsed in 0.1 M PBS, and then blocked for 1 h in 0.1 M PBS containing 0.3% Triton X-100 and 3% BSA. Next, the sections were incubated overnight at 4°C with the primary antibody (polyclonal sheep anti-SOD1 antibody at 1:500) in 0.1 M PBS containing 0.3% Triton X-100 and 3% BSA. After washing in 0.1 M PBS, sections were incubated for 30 min with the secondary antibody (biotinylated anti-sheep IgG). Subsequently, incubation was performed for 30 min in 3% H_2O_2 to eliminate endogenous peroxidases. After amplification with avidin-biotin complex (ABC kit, Vector Laboratories), visualization of reaction products was done with 0.05 M TBS (pH 7.6) containing 1.25% DAB and 0.75% hydrogen peroxide.

For electron microscopy, samples of SK-N-SH cells expressing L84V SOD1 and spinal cords from transgenic SOD1 L84V mice were decolorized, rehydrated, and rinsed in 0.1 M PBS. The samples were further fixed and dehydrated. Then the samples were embedded directly in epoxy resin, sectioned, counterstained, and examined as described under electron microscopy section.

SUPPORTING INFORMATION

Figure S1 Cytosolic localization of SOD1 in wt SOD1 expressing cells under ER stress. (A-F, A′-F′) Analysis of localization of SOD1 on ER. WT SOD1-expressing SK-N-SH cells were incubated for 24 h without (A-F) or with 1 ug/ml of tunicamycin (A′-F′). Then the cells were fixed and stained using an anti-SOD1 antibody (green; A, D, A′, D′) and an anti-KDEL antibody (red; B, B′) or an anti-GRP78 antibody (red; E, E′). GFP-cytochrome b5 were transfected to the cells and stained with anti-GFP (green; G, G′) and anti-SOD1 (red; H, H′) antibodies. Merged images (C, F, I, C′ F′, I′). (J-R, J′-R′) Analysis of SOD1 localization to the mitochondria. WT SOD1-expressing SK-N-SH cells were treated as described in above. The locations of the mitochondria and SOD1 were visualized in WT SOD1-expressing SK-N-SH cells using 100 nM Mito-tracker (red; K, K′), an anti-Tim17 antibody (red; N, N′) or an anti-Tom20 antibody (red; Q, Q′) and an anti-SOD1 antibody (green; J, M, P, J′, M′, P′). Merged images (L, O, R, L′, O′, R′). (S-U, S′-U′) Investigation of SOD1 localization to the Golgi apparatus. L84V SOD1-expressing SK-N-SH cells were treated as described in above. Then the cells were stained with anti-SOD1 antibody (green; S, S′) and anti-GM130 antibody (red; T, T′). Merged images (U, U′). (V-X, V′-X′) Analysis of the localization of SOD1 to the lysosomes. A GFP-tagged WT SOD1 vector was transfected into WT SOD1-expressing SK-N-SH cells. After 24 h of incubation with 1 ug/ml of tunicamycin, the cells were incubated for a further 30 min with 100 nM Lyso-tracker (red; W, W′) to visualize the lysosomes. GFP channel (V, V′) Merged images (X, X′). Scale bars = 20 um.
Found at: doi:10.1371/journal.pone.0001030.s001 (3.70 MB TIF)

ACKNOWLEDGMENTS

We are grateful to Dr. Otera and Prof. Mihara (Kyusyu University, Graduate School of Medical Science) and Dr. J. Niwa and Prof. G. Sobue (Nagoya University, Graduate School of Medicine) for providing anti-Tim17 and anti-Tom20 antibodies and myc-tagged ubiquitin expression vector, respectively. We thank Dr. K. Oono, Dr. S. Matsuda and Dr. T. Kudo (Osaka University, Graduate School of Medicine) for discussion and valuable advice. We thank Dr. George Wilkinson (Max-Planck Institute of Neurobiology) for critically reading the manuscript.

Author Contributions

Conceived and designed the experiments: SY YK TK SK MT. Performed the experiments: SY YK TK MT. Analyzed the data: SY YK TK MT JH MK MA YI SK MT. Contributed reagents/materials/analysis tools: SY YK TK MK MA YI. Wrote the paper: SY YK TK SK MT.

REFERENCES

1. Gurney ME (2000) What transgenic mice tell us about neurodegenerative disease. Bioessays 22: 297–304.
2. Brown RH Jr., Robberecht W (2001) Amyotrophic lateral sclerosis: pathogenesis. Semin Neurol 21: 131–139.
3. Cleveland DW, Rothstein JD (2001) From Charcot to Lou Gehrig: deciphering selective motor neuron death in ALS. Nat Rev Neurosci 2: 806–819.
4. Rowland LP, Shneider NA (2001) Amyotrophic lateral sclerosis. N Engl J Med 344: 1688–1700.
5. Julien JP (2001) Amyotrophic lateral sclerosis. unfolding the toxicity of the misfolded. Cell 104: 581–591.
6. Bruijn LI, Miller TM, Cleveland DW (2004) Unraveling the mechanisms involved in motor neuron degeneration in ALS. Annu Rev Neurosci 27: 723–749.
7. Rosen DR, Siddique T, Patterson D, Figlewicz DA, Sapp P, et al. (1993) Mutations in Cu/Zn superoxide dismutase gene are associated with familial amyotrophic lateral sclerosis. Nature 362: 59–62.
8. Forman MS, Lee VM, Trojanowski JQ (2003) 'Unfolding' pathways in neurodegenerative disease. Trends Neurosci 26: 407–410.
9. Kaufman RJ (2002) Orchestrating the unfolded protein response in health and disease. J Clin Invest 110: 1389–1398.
10. Tirasophon W, Welihinda AA, Kaufman RJ (1998) A stress response pathway from the endoplasmic reticulum to the nucleus requires a novel bifunctional protein kinase/endoribonuclease (Ire1p) in mammalian cells. Genes Dev 12: 1812–1824.
11. Wang B, Nguyen M, Breckenridge DG, Stojanovic M, Clemons PA, et al. (2003) Uncleaved BAP31 in association with A4 protein at the endoplasmic reticulum is an inhibitor of Fas-initiated release of cytochrome c from mitochondria. J Biol Chem 278: 14461–14468.
12. Bonifacino JS, Weissman AM (1998) Ubiquitin and the control of protein fate in the secretory and endocytic pathways. Annu Rev Cell Dev Biol 14: 19–57.
13. Travers KJ, Patil CK, Wodicka L, Lockhart DJ, Weissman JS, et al. (2000) Functional and genomic analyses reveal an essential coordination between the unfolded protein response and ER-associated degradation. Cell 101: 249–258.
14. Urano F, Wang X, Bertolotti A, Zhang Y, Chung P, et al. (2000) Coupling of stress in the ER to activation of JNK protein kinases by transmembrane protein kinase IRE1. Science 287: 664–666.
15. Nakagawa T, Yuan J (2000) Cross-talk between two cysteine protease families. Activation of caspase-12 by calpain in apoptosis. J Cell Biol 150: 887–894.
16. Nakagawa T, Zhu H, Morishima N, Li E, Xu J, et al. (2000) Caspase-12 mediates endoplasmic-reticulum-specific apoptosis and cytotoxicity by amyloid-beta. Nature 403: 98–103.
17. Katayama T, Imaizumi K, Sato N, Miyoshi K, Kudo T, et al. (1999) Presenilin-1 mutations downregulate the signalling pathway of the unfolded-protein response. Nat Cell Biol 1: 479–485.
18. Katayama T, Imaizumi K, Honda A, Yoneda T, Kudo T, et al. (2001) Disturbed activation of endoplasmic reticulum stress transducers by familial Alzheimer's disease-linked presenilin-1 mutations. J Biol Chem 276: 43446–43454.

19. Dickson KM, Bergeron JJ, Shames I, Colby J, Nguyen DT, et al. (2002) Association of calnexin with mutant peripheral myelin protein-22 ex vivo: a basis for "gain-of-function" ER diseases. Proc Natl Acad Sci U S A 99: 9852–9857.
20. Nishitoh H, Matsuzawa A, Tobiume K, Saegusa K, Takeda K, et al. (2002) ASK1 is essential for endoplasmic reticulum stress-induced neuronal cell death triggered by expanded polyglutamine repeats. Genes Dev 16: 1345–1355.
21. Takahashi R, Imai Y (2003) Pael receptor, endoplasmic reticulum stress, and Parkinson's disease. J Neurol 250 Suppl 3: III25–29.
22. Takahashi R, Imai Y, Hattori N, Mizuno Y (2003) Parkin and endoplasmic reticulum stress. Ann N Y Acad Sci 991: 101–106.
23. Hitomi J, Katayama T, Eguchi Y, Kudo T, Taniguchi M, et al. (2004) Involvement of caspase-4 in endoplasmic reticulum stress-induced apoptosis and Abeta-induced cell death. J Cell Biol 165: 347–356.
24. Kato S, Takikawa M, Nakashima K, Hirano A, Cleveland DW, et al. (2000) New consensus research on neuropathological aspects of familial amyotrophic lateral sclerosis with superoxide dismutase 1 (SOD1) gene mutations: inclusions containing SOD1 in neurons and astrocytes. Amyotroph Lateral Scler Other Motor Neuron Disord 1: 163–184.
25. Kato S, Horiuchi S, Liu J, Cleveland DW, Shibata N, et al. (2000) Advanced glycation endproduct-modified superoxide dismutase-1 (SOD1)-positive inclusions are common to familial amyotrophic lateral sclerosis patients with SOD1 gene mutations and transgenic mice expressing human SOD1 with a G85R mutation. Acta Neuropathol (Berl) 100: 490–505.
26. Kato S, Saito M, Hirano A, Ohama E (1999) Recent advances in research on neuropathological aspects of familial amyotrophic lateral sclerosis with superoxide dismutase 1 gene mutations: neuronal Lewy body-like hyaline inclusions and astrocytic hyaline inclusions. Histol Histopathol 14: 973–989.
27. Hirano A, Kurland LT, Sayre GP (1967) Familial amyotrophic lateral sclerosis. A subgroup characterized by posterior and spinocerebellar tract involvement and hyaline inclusions in the anterior horn cells. Arch Neurol 16: 232–243.
28. Wate R, Ito H, Zhang JH, Ohnishi S, Nakano S, et al. (2005) Expression of an endoplasmic reticulum-resident chaperone, glucose-regulated stress protein 78, in the spinal cord of a mouse model of amyotrophic lateral sclerosis. Acta Neuropathol (Berl) 110: 557–562.
29. Aoki M, Abe K, Houi K, Ogasawara M, Matsubara Y, et al. (1995) Variance of age at onset in a Japanese family with amyotrophic lateral sclerosis associated with a novel Cu/Zn superoxide dismutase mutation. Ann Neurol 37: 676–679.
30. Shibata N, Hirano A, Kobayashi M, Siddique T, Deng HX, et al. (1996) Intense superoxide dismutase-1 immunoreactivity in intracytoplasmic hyaline inclusions of familial amyotrophic lateral sclerosis with posterior column involvement. J Neuropathol Exp Neurol 55: 481–490.
31. Bruijn LI, Becher MW, Lee MK, Anderson KL, Jenkins NA, et al. (1997) ALS-linked SOD1 mutant G85R mediates damage to astrocytes and promotes rapidly progressive disease with SOD1-containing inclusions. Neuron 18: 327–338.
32. Niwa J, Ishigaki S, Hishikawa N, Yamamoto M, Doyu M, et al. (2002) Dorfin ubiquitylates mutant SOD1 and prevents mutant SOD1-mediated neurotoxicity. J Biol Chem 277: 36793–36798.
33. Urushitani M, Kurisu J, Tateno M, Hatakeyama S, Nakayama K, et al. (2004) CHIP promotes proteasomal degradation of familial ALS-linked mutant SOD1 by ubiquitinating Hsp/Hsc70. J Neurochem 90: 231–244.
34. Higgins CM, Jung C, Ding H, Xu Z (2002) Mutant Cu, Zn superoxide dismutase that causes motoneuron degeneration is present in mitochondria in the CNS. J Neurosci 22: RC215.
35. Tobisawa S, Hozumi Y, Arawaka S, Koyama S, Wada M, et al. (2003) Mutant SOD1 linked to familial amyotrophic lateral sclerosis, but not wild-type SOD1, induces ER stress in COS7 cells and transgenic mice. Biochem Biophys Res Commun 303: 496–503.
36. Kikuchi H, Almer G, Yamashita S, Guegan C, Nagai M, et al. (2006) Spinal cord endoplasmic reticulum stress associated with a microsomal accumulation of mutant superoxide dismutase-1 in an ALS model. Proc Natl Acad Sci U S A 103: 6025–6030.
37. Sasaki S, Warita H, Abe K, Iwata M (2005) Impairment of axonal transport in the axon hillock and the initial segment of anterior horn neurons in transgenic mice with a G93A mutant SOD1 gene. Acta Neuropathol (Berl) 110: 48–56.
38. Kato S, Nakashima K, Horiuchi S, Nagai R, Cleveland DW, et al. (2001) Formation of advanced glycation end-product-modified superoxide dismutase-1 (SOD1) is one of the mechanisms responsible for inclusions common to familial amyotrophic lateral sclerosis patients with SOD1 gene mutation, and transgenic mice expressing human SOD1 gene mutation. Neuropathology 21: 67–81.
39. Taylor JP, Hardy J, Fischbeck KH (2002) Toxic proteins in neurodegenerative disease. Science 296: 1991–1995.
40. Hyun DH, Lee M, Halliwell B, Jenner P (2003) Proteasomal inhibition causes the formation of protein aggregates containing a wide range of proteins, including nitrated proteins. J Neurochem 86: 363–373.
41. Kato S, Horiuchi S, Nakashima K, Hirano A, Shibata N, et al. (1999) Astrocytic hyaline inclusions contain advanced glycation endproducts in familial amyotrophic lateral sclerosis with superoxide dismutase 1 gene mutation: immunohistochemical and immunoelectron microscopical analyses. Acta Neuropathol (Berl) 97: 260–266.
42. Kato S, Sumi-Akamaru H, Fujimura H, Sakoda S, Kato M, et al. (2001) Copper chaperone for superoxide dismutase co-aggregates with superoxide dismutase 1 (SOD1) in neuronal Lewy body-like hyaline inclusions: an immunohistochemical study on familial amyotrophic lateral sclerosis with SOD1 gene mutation. Acta Neuropathol (Berl) 102: 233–238.
43. Kato S, Saeki Y, Aoki M, Nagai M, Ishigaki A, et al. (2004) Histological evidence of redox system breakdown caused by superoxide dismutase 1 (SOD1) aggregation is common to SOD1-mutated motor neurons in humans and animal models. Acta Neuropathol (Berl) 107: 149–158.
44. Bassik MC, Scorrano L, Oakes SA, Pozzan T, Korsmeyer SJ (2004) Phosphorylation of BCL-2 regulates ER Ca(2+) homeostasis and apoptosis. Embo J 23: 1207–1216.
45. Wootz H, Hansson I, Korhonen L, Lindholm D (2006) XIAP decreases caspase-12 cleavage and calpain activity in spinal cord of ALS transgenic mice. Exp Cell Res 312: 1890–1898.
46. Wootz H, Hansson I, Korhonen L, Napankangas U, Lindholm D (2004) Caspase-12 cleavage and increased oxidative stress during motoneuron degeneration in transgenic mouse model of ALS. Biochem Biophys Res Commun 322: 281–286.
47. Ishihara N, Mihara K (1998) Identification of the protein import components of the rat mitochondrial inner membrane, rTIM17, rTIM23, and rTIM44. J Biochem (Tokyo) 123: 722–732.
48. Kanaji S, Iwahashi J, Kida Y, Sakaguchi M, Mihara K (2000) Characterization of the signal that directs Tom20 to the mitochondrial outer membrane. J Cell Biol 151: 277–288.
49. Kato H, Sakaki K, Mihara K (2006) Ubiquitin-proteasome-dependent degradation of mammalian ER stearoyl-CoA desaturase. J Cell Sci 119: 2342–2353.

J Neuropathol Exp Neurol

Vol. 66, No. 11
November 2007
pp. 1037–1044

ORIGINAL ARTICLE

Intrathecal Delivery of Hepatocyte Growth Factor From Amyotrophic Lateral Sclerosis Onset Suppresses Disease Progression in Rat Amyotrophic Lateral Sclerosis Model

Aya Ishigaki, MD, PhD, Masashi Aoki, MD, PhD, Makiko Nagai, MD, PhD, Hitoshi Warita, MD, PhD, Shinsuke Kato, MD, PhD, Masako Kato, MD, PhD, Toshikazu Nakamura, PhD, Hiroshi Funakoshi, MD, PhD, and Yasuto Itoyama, MD, PhD

Abstract

Hepatocyte growth factor (HGF) is one of the most potent survival-promoting factors for motor neurons. We showed that introduction of the HGF gene into neurons of G93A transgenic mice attenuates motor neuron degeneration and increases the lifespan of these mice. Currently, treatment regimens using recombinant protein are closer to clinical application than gene therapy. To examine its protective effect on motor neurons and therapeutic potential we administered human recombinant HGF (hrHGF) by continuous intrathecal delivery to G93A transgenic rats at doses of 40 or 200 μg and 200 μg at 100 days of age (the age at which pathologic changes of the spinal cord appear, but animals show no clinical weakness) and at 115 days (onset of paralysis), respectively, for 4 weeks each. Intrathecal administration of hrHGF attenuates motor neuron degeneration and prolonged the duration of the disease by 63%, even with administration from the onset of paralysis. Our results indicated the therapeutic efficacy of continuous intrathecal administration of hrHGF in transgenic rats and should lead to the consideration for further clinical trials in amyotrophic lateral sclerosis using continuous intrathecal administration of hrHGF.

Key Words: Amyotrophic lateral sclerosis, Continuous intrathecal delivery, Hepatocyte growth factor, Neurodegeneration, Superoxide dismutase-1 (SOD1), Transgenic rat

From the Department of Neurology (AI, MA, MN, HW, YI), Tohoku University Graduate School of Medicine, Sendai, Japan; Tohoku University Hospital ALS Center (AI, MA, HW, YI), Sendai, Japan; Department of Neuropathology (SK), Institute of Neurological Sciences, Faculty of Medicine Tottori University, Yonago, Japan; Division of Pathology (MK), Tottori University Hospital, Yonago, Japan; and Division of Molecular Regenerative Medicine (TN, HF), Department of Biochemistry and Molecular Biology, Osaka University Graduate School of Medicine, Osaka, Japan.

Send correspondence and reprint requests to: Masashi Aoki, MD, PhD, Department of Neurology, Tohoku University Graduate School of Medicine, 1-1 Seiryo-machi, Sendai 980-8574, Japan; E-mail: aokim@mail.tains.tohoku.ac.jp

This work was supported by a grant from the Ministry of Health, Labor, and Welfare, Japan (YI, MA, SK, HF). Research funding was also provided by the Haruki ALS Research Foundation (YI, MA, HW) and by a Grant-in-Aid for Scientific Research from the Ministry of Education, Culture, Sports, Science, and Technology, Japan (MA, SK, HF).

INTRODUCTION

Amyotrophic lateral sclerosis (ALS) is a fatal neurodegenerative disease caused by selective motor neuron death (1). Approximately 10% of cases of ALS are inherited, usually as an autosomal dominant trait (2). In ~25% of familial cases, the disease is caused by mutations in the gene encoding cytosolic copper-zinc superoxide dismutase (SOD1) (3–5). The cause of ALS is still unclear, and clinical trials have as yet failed to identify any truly effective therapeutic regimens for ALS, with only riluzole providing a modest improvement in survival. Various substances have been shown to have therapeutic effects in a murine model of ALS. However, there have been a few reports of prolongation of survival with treatment starting around the time of disease onset (6–12).

We (13) and another group (14) developed a rat model of ALS expressing a human SOD1 transgene with 2 ALS-associated mutations: glycine to alanine at position 93 (G93A) and histidine to arginine at position 46 (H46R) (3, 5). Similar to its murine counterpart, this rat transgenic (Tg) ALS model reproduces the major phenotypic features of human ALS. Some experimental manipulations are difficult in Tg mice because of size limitations; however, this Tg rat model allows routine implantation of infusion pumps for intrathecal drug delivery. Intrathecal drug application is a well-established method for therapy and has been used in clinical trials in patients with ALS (15). This route of administration bypasses the blood-brain barrier, allowing rapid access to potential binding sites for the test compound in the spinal cord (16).

Hepatocyte growth factor (HGF) was first identified as a potent mitogen for mature hepatocytes and was first cloned in 1989 (17). Detailed studies indicated that HGF is expressed in the CNS (18) and is a novel neurotrophic factor (19, 20). HGF is one of the most potent survival-promoting factors for motor neurons, comparable to glial cell line-derived neurotrophic factor in vitro (21). Sun et al (22) reported that introduction of the HGF gene into neurons of G93A Tg mice attenuates motor neuron degeneration and increases the lifespan of these mice. Thus, HGF is a good candidate agent for treatment of ALS. Currently, treatment using recombinant protein is closer to clinical application than gene therapy. However, HGF has a very

short half-life (23–25) and shows poor penetration into the CNS. Therefore, we examined the effects of continuous intrathecal delivery of human recombinant HGF (hrHGF) into Tg rats using implanted infusion pumps for selective and less invasive supply of HGF to the spinal cord.

MATERIALS AND METHODS

Animal Preparation and Clinical Evaluation

G93A Tg rats were genotyped by polymerase chain reaction (PCR) assay using DNA obtained from the tail as described (13). To examine the dose and effects of hrHGF on disease onset, we began administration of 40 or 200 μg of hrHGF (provided by H. Funakoshi and T. Nakamura, Osaka University, Osaka, Japan) or vehicle (0.1 M sulfoxide PBS) for 4 weeks to groups of eight 100-day-old Tg rats, when the pathologic changes of the spinal cord appeared, but the animals did not show weakness. All animals were killed at 130 days by deep anesthesia, and the spinal cords were examined. Because treatment of patients with ALS patients is initiated only after diagnosis based on clinical signs and symptoms, we tested the effects of hrHGF on survival with administration beginning at around the age of onset of paralysis. We administered 200 μg of hrHGF or vehicle alone to groups of eight 115-day-old G93A Tg rats for 4 weeks, and the animals were observed until their death. To analyze the mechanism of action of hrHGF administration beginning at onset of paralysis we treated groups of six 115-day-old G93A Tg rats with 100 μg of hrHGF or with vehicle alone for 2 weeks (a dose comparable to 200 μg for 4 weeks). All rats were killed 2 weeks after commencement of administration of hrHGF, and their lumbar spinal cords were examined. Further groups of 3 G93A Tg rats and 3 non-Tg rats at 70, 100, and 130 days were used to measure the levels of rat HGF and c-Met. All rats were handled according to approved animal protocols of our institution and had free access to food and water throughout the experimental period and before and after pump implantation.

The onset of ALS was scored as the first observation of abnormal gait, evidence of limb weakness, or loss of extension of the hindlimbs when picked up at the base of the tail. We defined the appearance of paralysis as disease onset, although this is not a sensitive indicator and appears later than the decrease in activity (10). However, the appearance of paralysis is a suitable marker of disease onset because it is closer to the state at which patients will be diagnosed with the disease.

Footprints were collected every 3 days by letting the rats walk on a straight path after dipping their hind paws in black ink. We measured 3 strides within the area showing regular gait and calculated the means. Footprint measurements were made for rats that began treatment at 115 days. Examiners were blinded to which group each of the rats belonged in.

Preparation of the Osmotic Pumps and Transplant Surgery

Osmotic pumps (model number 2004 or 2002; Durect Corporation, Cupertino, CA) were incubated in sterile saline at 37°C for 40 hours to attain a constant flow rate before use. Pumps were filled to capacity with hrHGF solution or vehicle using a filling needle. An infusion tube was made by connecting a 1-cm length of polyethylene tubing (PE 60; Becton Dickinson, Franklin Lakes, NJ) to a small caliber tube 9 cm in length (PE 10; Becton Dickinson) using an adhesive (ARON ALPHA; Konishi Co., Osaka, Japan). The end of the infusion tube was connected to the shorter end of the flow moderator, the longer end of which was inserted into the pump.

Surgery for placement of the pump and intrathecal administration was performed as follows. Tg rats were anesthetized using diethyl ether and 1% halothane in a mixture of 30% oxygen and 70% nitrous oxide. The skin over the third to fifth lumbar spinal process was incised and the paravertebral muscles were separated from the vertebral lamina with scissors. The fifth lumbar vertebra was laminectomized, and the dura mater was exposed for insertion of the infusion tube. Particular care was taken not

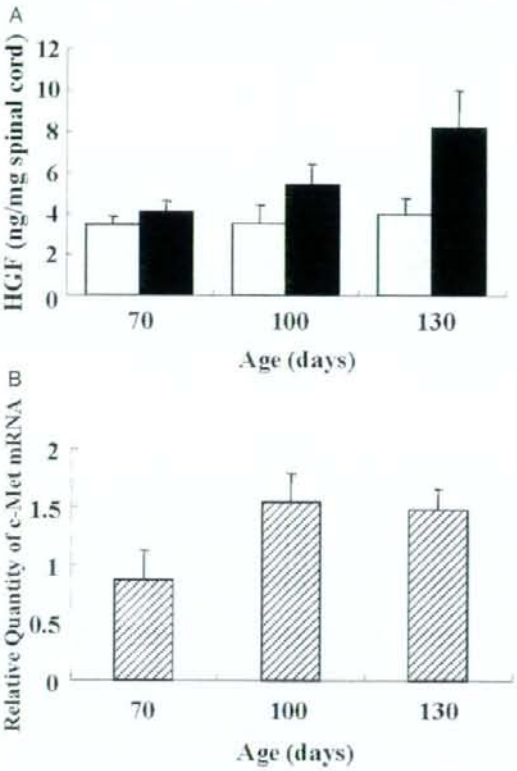

FIGURE 1. Increased levels of rat hepatocyte growth factor (HGF) and c-Met expression in the spinal cords of G93A transgenic (Tg) rats (n = 3) and non-Tg rats (n = 3). **(A)** Levels of endogenous rat HGF expression. Open bars, non-Tg rats; closed bars, G93A Tg rats. **(B)** Levels of c-Met mRNA of G93A Tg rats compared with non-Tg rats.

to injure the dura mater during laminectomy. A small hole was bored through the dura mater with a 24-gauge needle, and a polyethylene tube (PE 10, Becton Dickinson) was inserted into the subarachnoid space approximately 3 cm rostrally. A subcutaneous pocket was made into which the osmotic pump and pump side tube were implanted. The infusion tube was attached to the fascia over the paravertebral muscles at the incision margin with silk string. A drop of adhesive (ARON ALPHA) was applied, and the incision was closed by suturing the muscles and skin.

Measurement of Rat and Human HGF in the Lumbar Spinal Cord

Slices of the fifth lumbar cord from 3 G93A Tg rats and 3 non-Tg rats at 70, 100, and 130 days as well as from 130-day-old G93A Tg rats treated with 40 or 200 μg of hrHGF or vehicle alone for 4 weeks starting at 100 days were homogenized in buffer (20 mM Tris-HCl, pH 7.5, 0.1% Tween-80, 1 mM phenylmethylsulfonyl fluoride, and 1 mM EDTA) and centrifuged at 15,000 rpm for 30 minutes. Supernatants were separated and the concentrations of rat endogenous HGF were measured using an enzyme-linked immunosorbent assay (ELISA) kit, which is specific for rat HGF without detecting human HGF (22) (Institute of Immunology, Tokyo, Japan). For measurement of human HGF in the treated rats we used a human HGF-specific ELISA kit (IMMUNIS, Institute of Immunology), which is not reactive with rat HGF (26, 27).

Measurement of c-Met mRNA in the Lumbar Spinal Cord of Tg Rats

Aliquots of 1 μg of total RNA from the lumbar cords of rats were used as templates for synthesis of double-stranded cDNA. Real-time quantitative PCR was performed for c-Met and glyceraldehyde-3-phosphate dehydrogenase (GAPDH) [GAPDH forward primer, 5′-CCATCACTGCCACTCAGAAGAC-3′; GAPDH reverse primer, 5′-TCATACTTGGCAGGTTTCTCCA-3′; GAPDH TaqMan probe, 5′(FAM)-ACCACGAGCACTGTTTCAATAGGACCC-(TAMRA)3′; c-MET forward primer, 5′-GTACGGTGTCTCCAGCATTTTT-3′; c-Met reverse primer, 5′-AGAGCACCACCTGCATGAAG-3′; TaqMan probe, 5′(FAM)-CGTGTTCCTACCCCCAATGTATCCGT- (TAMRA)3′]. An ABI Prism 7700 Sequence Detection System (Applied Biosystems Perkin-Elmer, Foster City, CA) was used to monitor emission intensities using the above primer pairs and TaqMan fluorogenic probes. The c-Met mRNA level of G93A Tg rats relative to non-Tg rats was calculated using the Comparative C_T Method (Applied Biosystems).

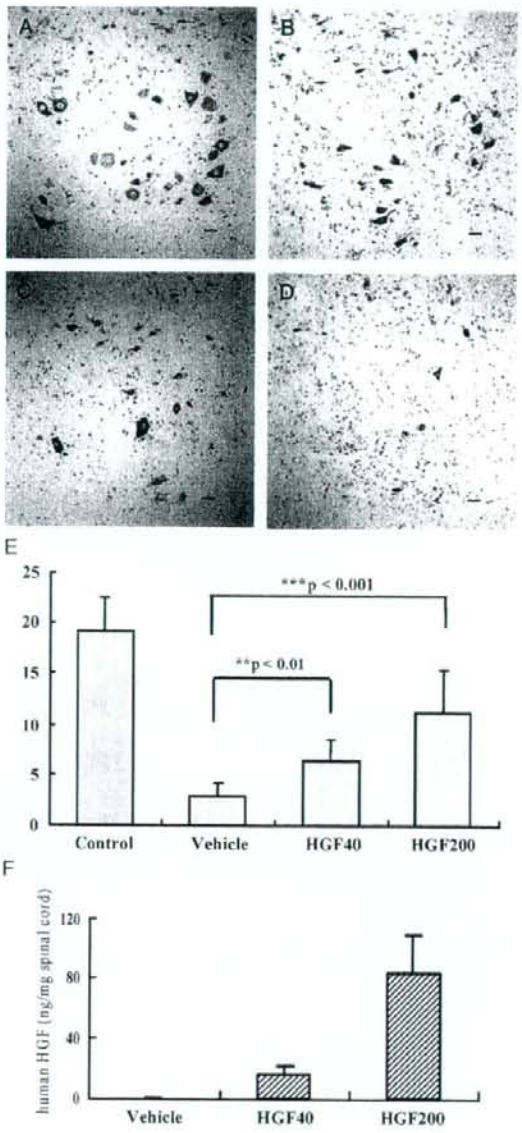

FIGURE 2. Intrathecal administration of hepatocyte growth factor (HGF) to G93A transgenic (Tg) rats at 100 days showed a protective effect against motor neuron death. **(A–D)** Histologic evaluation of the anterior horn with Nissl staining at 130 days: **(A)** lumbar cord of non-Tg rats; **(B)** 200 μg of human recombinant HGF (hrHGF)-treated; **(C)** 40 μg of hrHGF-treated; and **(D)** vehicle-treated G93A Tg rats. Scale bar = 40 μm. **(E)** Quantitative morphometric evaluation of surviving motor neurons of the fifth lumbar anterior horn at 130 days. We counted neurons that were >40 μm in diameter. Significantly larger numbers of motor neurons survived in hrHGF-treated G93A Tg rats ($p < 0.01$ and $p < 0.001$, 40 and 200 μg of hrHGF, respectively), compared with vehicle-treated G93A Tg rats ($n = 8$ in each group). **(F)** Levels of human HGF concentration in lumbar spinal cords of G93A Tg rats treated with 200 μg of hrHGF, 40 μg of hrHGF, and vehicle.

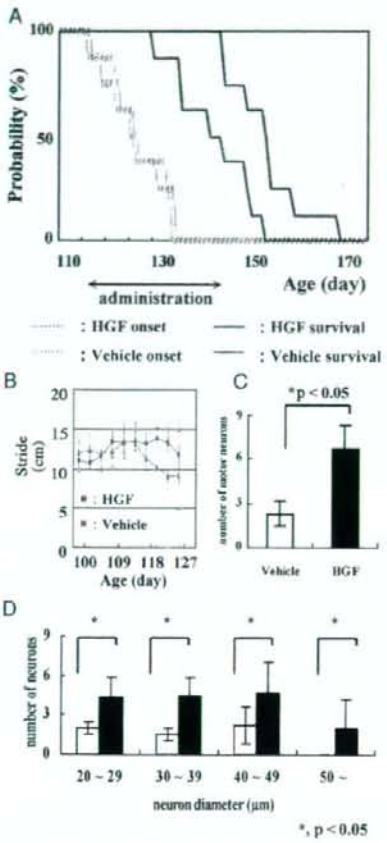

FIGURE 3. Intrathecal administration of hepatocyte growth factor (HGF) from 115 days (just before disease onset) retarded disease progression. **(A)** Survival periods were 143.25 ± 17.0 days in the vehicle-treated group (solid blue line) and 154.3 ± 16.4 days in the 200 μg of human recombinant HGF (hrHGF)-treated group (solid red line). Survival of hrHGF-treated animals was extended significantly ($p = 0.0135$), although there were no significant differences in onset (dotted lines, $n = 8$ in each group, $p = 0.6346$). **(B)** Footprint analysis demonstrated a delay in decline of stride length in G93A transgenic (Tg) rats treated with 200 μg of hrHGF relative to vehicle-treated G93A Tg rats (error bars, ± SD). **(C, D)** Quantitative morphometric evaluation of surviving motor neurons that were >40 μm in diameter **(C)** and neuron size distribution **(D)** in the fifth lumbar anterior horn of G93A Tg rats 2 weeks after administration from 115 days. Significantly larger number of motor neurons survived in the hrHGF-treated G93A Tg rats compared with vehicle-treated G93A Tg rats (6.7 ± 1.6 vs 2.3 ± 0.9; $p = 0.002$, $n = 6$ in each group) **(C)**.

Histopathologic and Immunohistochemical Analyses

To examine the dose and effects of hrHGF against disease onset, we began administration of 40 or 200 μg of hrHGF or vehicle alone to groups of eight 100-day-old Tg rats each for 4 weeks. At 130 days, G93A Tg rats were administered hrHGF or vehicle, and non-Tg rats were deeply anesthetized with diethyl ether and killed for histopathologic evaluation. To examine the effects of hrHGF administration beginning at onset of paralysis, 100 μg of HGF or vehicle alone was administered to groups of six 115-day-old Tg rats for 2 weeks. These animals were killed by deep anesthesia with diethyl ether 2 weeks after the operation. Under deep anesthesia these animals were perfused via the aorta with physiologic saline at 37°C and their lumbar spinal cords were removed. The fifth lumbar spinal cord tissue was embedded in OCT compound (Sakura Finetek Japan Co., Tokyo, Japan), frozen in an acetone/dry ice bath after fixation with 4% paraformaldehyde, and supplemented with 0.1 M cacodylate buffer (pH 7.3) containing 30% sucrose. Other spinal cord tissue specimens were frozen in dry ice and cut into frozen sections (12-μm-thick) and then washed with PBS. To evaluate the effects of HGF on motor neuron loss we compared the numbers of lumbar motor neurons in each group by counting as mentioned below. To evaluate the effects of HGF on apoptosis and to determine whether HGF receptors were activated, we compared the results of immunohistochemical staining of the lumbar cords for activated caspase-3, activated caspase-9 (Cell Signaling Technology, Inc., Beverly, MA), and phosphorylated c-Met (activated HGF receptor) (BioSource International, Camerillo, CA). The staining specificity of the antibodies was assessed by preabsorption of the primary antibody with excess peptide, omission of the primary antibody, or replacement of the primary antibody with normal rabbit IgG (22). We examined every seventh section from 42 serial sections of the fifth lumbar spinal cord. We counted neurons that had a clear nucleolus and were multipolar with neuronal morphology (13, 22), >40 μm in diameter, and located in a defined area of the anterior horn of the spinal cord. Cell counts were performed using ImageJ software (National Institutes of Health, Bethesda, MD) on images captured electronically (28).

Western Blotting

Lysates from the lumbar spinal cord of each rat were prepared in RIPA buffer (150 mM NaCl, 1% Nonidet P-40, 0.5% deoxycholate, 0.1% sodium dodecyl sulfate, and 50 mM Tris, pH 8.0). Equal amounts of proteins from the lysates (50 μg) were resolved by sodium dodecyl sulfate-polyacrylamide gel electrophoresis, transferred onto polyvinylidene diflouride membranes, and immunoblotted. The primary antibodies used were anti-caspase-3 (Sigma-Aldrich, St. Louis, MO), anti-caspase-9 (Stressgen Biotechnologies Corporation, Victoria, BC, Canada), anti-X-linked inhibitor of apoptosis protein (XIAP) (Cell Signaling Technology, Inc.), and anti-excitatory amino acid transporter 2 (EAAT2) antibodies (Chemicon International, Temecula, CA). After incubation of membranes with HRP-coupled

secondary antibodies, proteins were visualized using ECL or ECL Plus Western Blotting Detection Reagents (Amersham Biosciences Inc., Piscataway, NJ) and a Fluorochem image analyzer (LAS-3000 mini; Fuji Photo Film Co., Tokyo, Japan).

Statistical Analysis

The Kaplan-Meier and log-rank test were used for statistical analyses of differences in onset and survival between groups. For statistical analyses of differences in body weight, footprint, motor neuron cell count, and Western blotting we used analysis of variance and post hoc tests. The data are reported as means ± SD.

RESULTS

Measurement of the Levels of Rat HGF and c-Met Expression in Untreated Animals

Groups of 3 G93A Tg rats and non-Tg rats at 70, 100, and 130 days were used to measure the levels of rat HGF without any treatment. In the lumbar cords of untreated G93A Tg rats, the HGF concentrations increased with disease progression (Fig. 1A). At 70 days the level of rat HGF in the lumbar cords of G93A Tg rats was 4.05 ± 0.6 ng/mg and was the same as that of non-Tg rats. Increases of 35% and 107% were observed in the rat HGF level at 100 and 130 days, respectively, compared with non-Tg rats.

In addition, we measured the levels of c-Met mRNA in the lumbar spinal cords of Tg rats relative to non-Tg rats by real-time quantitative PCR. In the lumbar cords of G93A Tg rats the level of c-Met mRNA expression was the same as that in non-Tg rats at 70 days. However, a 55% increase in the level of c-Met mRNA expression compared with that of non-Tg rats was observed at 100 days and the higher level of expression was retained at 130 days (Fig. 1B).

Administration of hrHGF to 100-Day-Old G93A Tg Rats for 4 Weeks

To examine the efficacy of hrHGF on motor neurons in the spinal cords of Tg rats against onset of disease we administered 40 and 200 μg of hrHGF or vehicle alone to 100-day-old G93A Tg rats for 4 weeks (n = 8 in each group). Animals were killed at 130 days, and their lumbar spinal cords were examined. Because administration of hrHGF for more than 30 days may induce antibodies against hrHGF, we did not treat rats for longer than this period. We confirmed elevation of human HGF concentrations in the lumbar cords of hrHGF-treated rats using a specific sandwich immunoassay. The mean human HGF concentrations were 83.9 ± 25.1, 15.6 ± 5.4, and 0 ng/mg for rats treated with 200 μg of hrHGF, 40 μg of hrHGF, and vehicle, respectively (Fig. 2F). The endogenous rat HGF concentration is 4 to 5 ng/mg at this age (Fig. 1A). The human HGF concentration in the spinal cord of G93A Tg rats treated with 200 μg of hrHGF

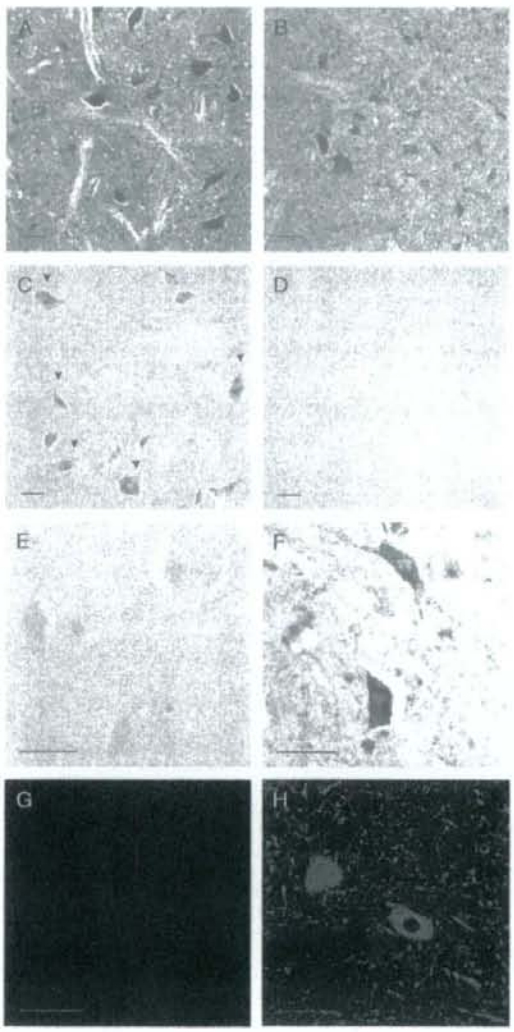

FIGURE 4. Sections of the fifth lumbar anterior horn from G93A transgenic (Tg) rats treated with human recombinant hepatocyte growth factor (hrHGF) **(A, C, E, G)** or vehicle **(B, D, F, H)** for 2 weeks starting at 115 days were stained with hematoxylin and eosin **(A, B)** and antibodies to phosphorylated c-Met **(C, D)**, activated caspase-3 **(E, F)**, and activated caspase-9 **(G, H)**. Scale bar = 50 μm. There were larger numbers of remaining large motor neurons in hrHGF-treated G93A Tg rats (6.7 ± 1.6) **(A)** than in vehicle-treated G93A Tg rats (2.3 ± 0.9) **(B)**. Phosphorylated c-Met staining was more distinct in hrHGF-treated G93A Tg rats **(C)** than in vehicle-treated G93A Tg rats **(D)**. In contrast, activated caspase-3 staining was stronger in vehicle-treated G93A Tg rats **(F)** than in hrHGF-treated G93A Tg rats **(E)**. Activated caspase-9 staining was detectable in vehicle-treated G93A Tg rats **(H)** compared with little reactivity in hrHGF-treated G93A Tg rats **(G)**.

was increased by approximately 20-fold relative to the endogenous rat HGF. All vehicle-treated G93A Tg rats developed weakness in the hindlimbs with a mean onset of 118.8 ± 4.3 days. Seven of 8 G93A Tg rats treated with 40 μg of rhHGF developed the disease before 130 days. In contrast, only 3 of 8 animals treated with 200 μg of rhHGF developed paralysis before this stage. At 130 days the average numbers of motor neurons in the ventral horn were as follows: non-Tg rats, 19.2 ± 3.3; vehicle only, 2.9 ± 1.3; 40 μg of hrHGF, 6.3 ± 2.1; and 200 μg of hrHGF, 11.2 ± 4.2. Significantly more motor neurons survived in hrHGF-treated (40 μg, $p < 0.01$; 200 μg, $p < 0.001$) than in vehicle-treated G93A Tg rats (Fig. 2A–E). hrHGF prevented motor neuron death in G93A Tg rats in a dose-dependent manner.

Administration of hrHGF to 115-Day-Old G93A Tg Rats for 4 Weeks

We next examined the therapeutic potential of HGF when administration was started at around the age of onset of paralysis. We administered 200 μg of hrHGF or vehicle alone to 115-day-old G93A Tg rats for 4 weeks. There were no statistically significant differences ($p = 0.6346$) in onset between the groups (200 μg of hrHGF, 126.8 ± 13.1 days; vehicle, 126.3 ± 13.8 days) (Fig. 3A, dotted lines). In contrast, 200 μg of hrHGF extended mean survival by 11 days compared with vehicle-treated G93A Tg rats ($p = 0.0135$) (Fig. 3A, solid lines), although G93A Tg rats showed very rapid disease progression and died within 20 days of disease onset. The average periods from the onset to death were 16.9 ± 8.17 and 27.5 ± 11.1 days in vehicle ($n = 8$) and hrHGF ($n = 8$) groups, respectively. The latter represented an increase of 62.7% relative to vehicle-treated controls. Footprint analysis of stride length in 200 μg of hrHGF-treated G93A Tg rats showed significant improvement compared with vehicle-treated G93A Tg rats at 118 days ($p = 0.0424$) (Fig. 3B). Thus, despite the very rapid disease progression in this model and short treatment period of 4 weeks, hrHGF treatment improved motor performance and prolonged survival even with treatment beginning around the onset of paralysis.

Histologic evaluation of the lumbar spinal cord indicated that hrHGF treatment prevented the pathologic changes typical of Tg rats. Two weeks after commencement of administration at 129 days, vehicle-treated rats showed substantial loss of motor neurons (2.3 ± 0.9) compared with hrHGF-treated rats (6.6 ± 1.6) (Figs. 3C, 4A, B). A significantly larger number of motor neurons survived in hrHGF-treated G93A Tg rats than in vehicle-treated G93A Tg rats ($p = 0.002$). Histologic evaluation of the lumbar spinal cord revealed much greater numbers of phosphorylated c-Met-positive cells (which were presumed to be motor neurons because of their large size, multipolar form, and localization in the anterior horn of the spinal cord) in hrHGF-treated G93A Tg rats compared with vehicle-treated G93A Tg rats at 2 weeks after the start of administration at 129 days (Fig. 4C, D). These observations indicated that the administered hrHGF was used in the spinal cord in G93A Tg rats. Consistent with the observation that apoptosis is involved in the pathogenesis of ALS (29–32), immunohistochemical analyses indicated large numbers of cells positive for activated caspase-3 and caspase-9 in vehicle-treated rats (Fig. 4F, H), compared with little or no reactivity in hrHGF-treated rats (Fig. 4E, G). To assess the mechanisms of suppression of caspase-3 and caspase-9 activation in hrHGF-treated rats, we next examined the level of XIAP by Western blotting, as XIAP inhibits activation of these pro-caspases and its levels are decreased in ALS mice (31). Western blotting analysis revealed increased XIAP expression

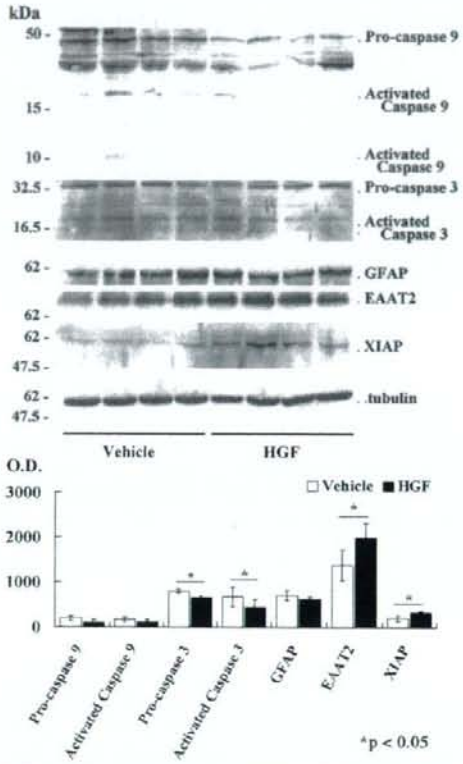

FIGURE 5. Caspase-3 and -9, glial fibrillary acidic protein (GFAP), excitatory amino acid transporter 2 (EAAT2), X-linked inhibitor of apoptosis protein (XIAP), and β-tubulin expression in the lumbar spinal cord. Western blotting of lumbar spinal cord lysates from G93A transgenic (Tg) rats treated with 100 μg of human recombinant hepatocyte growth factor (hrHGF) or vehicle for 2 weeks from 115 days. Western blotting analysis revealed increased levels of EAAT2 and XIAP expression in the spinal cords of hrHGF-treated G93A Tg rats compared with vehicle-treated G93A Tg rats (XIAP, $p = 0.0099$; EAAT2, $p = 0.0417$; $n = 4$). On the other hand, activated caspase-3 and -9 expression levels were decreased in hrHGF-treated G93A Tg rats. There were significant differences in caspase-3 expression between hrHGF- and vehicle-treated G93A Tg rats (pro-caspase-3, $p = 0.0031$; activated caspase-3, 0.0154; $n = 4$). GFAP expression was equivalent in both groups.

in the spinal cord of G93A Tg rats, and the increase in hrHGF-treated rats was only 60% of that in vehicle-treated G93A Tg rats. On the other hand, activated caspase-3 and 9 levels were decreased in hrHGF-treated G93A Tg rats ($p = 0.0154$ and $p = 0.2364$, 75% and 69% of vehicle-treated G93A Tg rats, respectively). These were all considered to be effects of HGF on motor neurons. Finally, we examined whether HGF improves the function of other cell types, such as astrocytes. There was a 60% increase in glial-specific glutamate transporter (EAAT2) in hrHGF-treated rats compared with vehicle-treated controls, although there was little difference in GFAP expression levels between the 2 groups (Fig. 5).

DISCUSSION

In this study, we demonstrated dose-dependent effects of hrHGF on motor neurons in the G93A Tg rat model of ALS, with administration starting at 100 days. Furthermore, we showed that hrHGF retards disease progression in this animal model treated from 115 days at the time of disease onset. There have been many studies of possible treatments in a mouse model of ALS (33, 34), but few agents have been shown to prolong survival with administration starting around disease onset (6–12). In this study, recombinant hrHGF retarded disease development even with administration beginning around the age onset of paralysis. Here, we showed the therapeutic effects of intrathecal delivery of a neurotrophic factor as a protein, rather than a transgene, on ALS beginning at the onset of paralysis. The average survival period of hrHGF-treated rats was 62.7% longer than that of vehicle-treated controls, comparable with the improved survival obtained by viral delivery of insulin-like growth factor-1 (6). We defined the appearance of paralysis as disease onset, although this is not a sensitive indicator and appears later than the decrease in activity (10). However, the appearance of paralysis is a clinically relevant marker of disease onset because it is closer to the state at which patients will be diagnosed with the disease.

We confirmed elevation of the human HGF concentration in the lumbar cords of hrHGF-treated G93A Tg rats using a specific sandwich immunoassay. Histologic evaluation of the lumbar spinal cord revealed greater numbers of phosphorylated c-Met-positive motor neurons in hrHGF-treated G93A Tg rats. This finding suggested that HGF receptors of motor neurons were activated well by administered hrHGF (35). These observations indicated that the administered hrHGF penetrated into the spinal cord and was utilized in the motor neurons of spinal cord. Previous studies demonstrated that many trophic factors have protective effects on motor neurons. In human trials of neurotrophic factors, such as brain-derived neurotrophic factors, glial cell line-derived neurotrophic factor, and insulin-like growth factor-1, the delivery (accessibility) of the protein to the motor neurons and glia in the spinal cord has been argued to be essential. Our results confirmed that chronic intrathecal administration with implanted infusion pumps supplied appropriate therapeutic doses to spinal cord motor neurons.

The HGF concentrations in cerebrospinal fluid are increased in many neurologic disorders, including ALS (26). In G93A Tg rats, the level of endogenous HGF in the spinal cord showed significantly greater elevation when the pathologic changes began in the spinal cord and increased with progression of the disease compared with the level of endogenous HGF in the spinal cord of non-Tg rats. After onset, the level of endogenous HGF almost doubled relative to that in non-Tg rats (Fig. 1A). These results were compatible to observations in patients with sporadic as well as familial ALS (36, 37). The level of c-met RNA expression in the lumbar cord of G93A rats increased to 155% of the normal level from before onset, and this elevated expression was retained after onset of disease (Fig. 1B). Kato et al (36) demonstrated that autocrine and paracrine trophic support of the HGF-c-met system contributes to attenuation of the degeneration of residual spinal cord motor neurons in ALS, whereas disruption of the HGF-c-met system at an advanced stage of disease accelerates cellular degeneration (37). Administration of hrHGF delayed the pathologic changes in G93A Tg rats. This effect of HGF may be due to replenishment of the relative insufficiency of HGF in G93A Tg rats in the present study.

Consistent with the findings that apoptosis is involved in ALS (29–31), large numbers of cells immunopositive for activated caspase-3 and -9 were observed in vehicle-treated animals in contrast to little or no reactivity in hrHGF-treated rats. This result was verified by quantitative Western blotting analysis, which indicated that HGF could block caspase activation of apoptosis. Caspase-3 and -9 are the main factors involved in execution of the caspase cascade. The survival-prolonging effect of HGF may be explained by suppression of induction and activation of caspase-9, as this enzyme is involved in determining disease duration (31). These observations suggest that the mechanism of the therapeutic effect of HGF in G93A Tg rats includes inhibition of the caspase cascade or of the cell death mechanism preceding the caspase cascade. In addition, EAAT2 and XIAP expression levels were increased in the hrHGF-treated group compared with vehicle-treated controls, indicating that HGF affected not only motor neurons via inhibition of the caspase cascade but also other cell types, such as astrocytes, which support motor neurons by maintaining or reinforcing internal cell protective functions, such as EAAT2 and XIAP.

Our results demonstrate pathologic improvements and retarded progression of ALS in G93A Tg rats by intrathecal administration of hrHGF from around the time of disease onset. Because HGF and c-Met are thought to be regulated in cases of not only familial but also sporadic ALS in a manner similar to the Tg mouse model of ALS (36), our findings suggest the possibility of clinical use of HGF in both familial and sporadic ALS. The results indicating the efficiency of hrHGF administration even from the onset of paralysis should prompt further clinical trials in ALS.

ACKNOWLEDGMENT

We thank Rieko Kamii for technical assistance.

REFERENCES

1. Rowland LP. Amyotrophic lateral sclerosis. Curr Opin Neurol 1994;7: 310–15
2. Mulder DW, Kurland LT, Offord KP, et al. Familial adult motor neuron disease: Amyotrophic lateral sclerosis. Neurology 1986;36:511–17

3. Rosen DR. Mutations in Cu/Zn superoxide dismutase gene are associated with familial amyotrophic lateral sclerosis. Nature 1993; 364:362
4. Deng HX, Hentati A, Tainer JA, et al. Amyotrophic lateral sclerosis and structural defects in Cu,Zn superoxide dismutase. Science 1993;261: 1047–51
5. Aoki M, Ogasawara M, Matsubara Y, et al. Mild ALS in Japan associated with novel SOD mutation. Nat Genet 1993;5:323–24
6. Kaspar BK, Llado J, Sherkat N, et al. Retrograde viral delivery of IGF-1 prolongs survival in a mouse ALS model. Science 2003;301:839–42
7. Azzouz M, Ralph GS, Storkebaum E, et al. VEGF delivery with retrogradely transported lentivector prolongs survival in a mouse ALS model. Nature 2004;429:413–17
8. Kieran D, Kalmar B, Dick JR, et al. Treatment with arimoclomol, a coinducer of heat shock proteins, delays disease progression in ALS mice. Nat Med 2004;10:402–5
9. Rothstein JD, Patel S, Regan MR, et al. β-Lactam antibiotics offer neuroprotection by increasing glutamate transporter expression. Nature 2005;433:73–77
10. Storkebaum E, Lambrechts D, Dewerchin M, et al. Treatment of motoneuron degeneration by intracerebroventricular delivery of VEGF in a rat model of ALS. Nat Neurosci 2005;8:85–92
11. Wu AS, Kiaei M, Aguirre N, et al. Iron porphyrin treatment extends survival in a transgenic animal model of amyotrophic lateral sclerosis. J Neurochem 2003;85:142–50
12. Crow JP, Calingasan NY, Chen J, et al. Manganese porphyrin given at symptom onset markedly extends survival of ALS mice. Ann Neurol 2005;58:258–65
13. Nagai M, Aoki M, Miyoshi I, et al. Rats expressing human cytosolic copper-zinc superoxide dismutase transgenes with amyotrophic lateral sclerosis: Associated mutations develop motor neuron disease. J Neurosci 2001;21:9246–54
14. Howland DS, Liu J, She Y, et al. Focal loss of the glutamate transporter EAAT2 in a transgenic rat model of SOD1 mutant-mediated amyotrophic lateral sclerosis (ALS). Proc Natl Acad Sci USA 2002;99: 1604–9
15. Ochs G, Penn RD, York M, et al. A phase I/II trial of recombinant methionyl human brain derived neurotrophic factor administered by intrathecal infusion to patients with amyotrophic lateral sclerosis. Amyotroph Lateral Scler Other Motor Neuron Disord 2000;1:201–6
16. Ochs G, Giess R, Bendszus M, et al. Epi-arachnoidal drug deposit: A rare complication of intrathecal drug therapy. J Pain Symptom Manage 1999;18:229–32
17. Nakamura T, Nishizawa T, Hagiya M, et al. Molecular cloning and expression of human hepatocyte growth factor. Nature 1989;342: 440–43
18. Jung W, Castren E, Odenthal M, et al. Expression and functional interaction of hepatocyte growth factor-scatter factor and its receptor c-met in mammalian brain. J Cell Biol 1994;126:485–94
19. Matsumoto K, Nakamura T. HGF: Its organotrophic role and therapeutic potential. Ciba Found Symp 1997;212:198–211, discussion 11–14
20. Maina F, Klein R. Hepatocyte growth factor, a versatile signal for developing neurons. Nat Neurosci 1999;2:213–17
21. Ebens A, Brose K, Leonardo ED, et al. Hepatocyte growth factor/scatter factor is an axonal chemoattractant and a neurotrophic factor for spinal motor neurons. Neuron 1996;17:1157–72
22. Sun W, Funakoshi H, Nakamura T. Overexpression of HGF retards disease progression and prolongs life span in a transgenic mouse model of ALS. J Neurosci 2002;22:6537–48
23. Liu KX, Kato Y, Narukawa M, et al. Importance of the liver in plasma clearance of hepatocyte growth factors in rats. Am J Physiol 1992;263: G642–49
24. Appasamy R, Tanabe M, Murase N, et al. Hepatocyte growth factor, blood clearance, organ uptake, and biliary excretion in normal and partially hepatectomized rats. Lab Invest 1993;68:270–76
25. Liu KX, Kato Y, Kino I, et al. Ligand-induced downregulation of receptor-mediated clearance of hepatocyte growth factor in rats. Am J Physiol 1998;275:E835–42
26. Funakoshi H, Nakamura T. Hepatocyte growth factor: From diagnosis to clinical applications. Clin Chim Acta 2003;327:1–23
27. Hayashi Y, Kawazoe Y, Sakamoto T, et al. Adenoviral gene transfer of hepatocyte growth factor prevents death of injured adult motoneurons after peripheral nerve avulsion. Brain Res 2006;1111:187–95
28. Grondard C, Biondi O, Armand AS, et al. Regular exercise prolongs survival in a type 2 spinal muscular atrophy model mouse. J Neurosci 2005;25:7615–22
29. Li M, Ona VO, Guegan C, et al. Functional role of caspase-1 and caspase-3 in an ALS transgenic mouse model. Science 2000;288: 335–39
30. Friedlander RM, Brown RH, Gagliardini V, et al. Inhibition of ICE slows ALS in mice. Nature 1997;388:31
31. Inoue H, Tsukita K, Iwasato T, et al. The crucial role of caspase-9 in the disease progression of a transgenic ALS mouse model. EMBO J 2003; 22:6665–74
32. Pasinelli P, Houseweart MK, Brown RH Jr. Caspase-1 and -3 are sequentially activated in motor neuron death in Cu,Zn superoxide dismutase-mediated familial amyotrophic lateral sclerosis. Proc Natl Acad Sci USA 2000;97:13901–6
33. Gurney ME, Pu H, Chiu AY, et al. Motor neuron degeneration in mice that express a human Cu,Zn superoxide dismutase mutation. Science 1994;264:1772–75
34. Gurney ME, Cutting FB, Zhai P, et al. Benefit of vitamin E, riluzole, and gabapentin in a transgenic model of familial amyotrophic lateral sclerosis. Ann Neurol 1996;39:147–57
35. Machide M, Hashigasako A, Matsumoto K, et al. Contact inhibition of hepatocyte growth regulated by functional association of the c-Met/hepatocyte growth factor receptor and LAR protein-tyrosine phosphatase. J Biol Chem 2006;281:8765–72
36. Kato S, Funakoshi H, Nakamura T, et al. Expression of hepatocyte growth factor and c-Met in the anterior horn cells of the spinal cord in the patients with amyotrophic lateral sclerosis (ALS): Immunohistochemical studies on sporadic ALS and familial ALS with superoxide dismutase 1 gene mutation. Acta Neuropathol (Berl) 2003;106:112–20
37. Jiang YM, Yamamoto M, Kobayashi Y, et al. Gene expression profile of spinal motor neurons in sporadic amyotrophic lateral sclerosis. Ann Neurol 2005;57:236–51

WILEY InterScience

Journal of Neuroscience Research 85:2332–2342 (2007)

Hepatocyte Growth Factor Promotes Endogenous Repair and Functional Recovery After Spinal Cord Injury

Kazuya Kitamura,[1,2] Akio Iwanami,[1–3] Masaya Nakamura,[1] Junichi Yamane,[1,2] Kota Watanabe,[1] Yoshinori Suzuki,[4] Daisuke Miyazawa,[4] Shinsuke Shibata,[2] Hiroshi Funakoshi,[4] Shinichi Miyatake,[5] Robert S. Coffin,[6] Toshikazu Nakamura,[4] Yoshiaki Toyama,[1] and Hideyuki Okano[2]*

[1]Department of Orthopaedic Surgery, Keio University School of Medicine, Shinjuku, Tokyo, Japan
[2]Department of Physiology, Keio University School of Medicine, Shinjuku, Tokyo, Japan
[3]Clinical Research Center, National Hospital Organization, Murayama Medical Center, Musashimurayama, Tokyo, Japan
[4]Division of Molecular Regenerative Medicine, Osaka University Graduate School of Medicine, Suita, Osaka, Japan
[5]Department of Neurosurgery, Osaka Medical College, Takatsuki, Osaka, Japan
[6]Department of Molecular Pathology, Windeyer Institute of Medical Science of University College, London, United Kingdom

Many therapeutic interventions using neurotrophic factors or pharmacological agents have focused on secondary degeneration after spinal cord injury (SCI) to reduce damaged areas and promote axonal regeneration and functional recovery. Hepatocyte growth factor (HGF), which was identified as a potent mitogen for mature hepatocytes and a mediator of inflammatory responses to tissue injury, has recently been highlighted as a potent neurotrophic and angiogenic factor in the central nervous system (CNS). In the present study, we revealed that the extent of endogenous HGF up-regulation was less than that of c-Met, an HGF receptor, during the acute phase of SCI and administered exogenous HGF into injured spinal cord using a replication-incompetent herpes simplex virous-1 (HSV-1) vector to determine whether HGF exerts beneficial effects and promotes functional recovery after SCI. This treatment resulted in the significant promotion of neuron and oligodendrocyte survival, angiogenesis, axonal regrowth, and functional recovery after SCI. These results suggest that HGF gene delivery to the injured spinal cord exerts multiple beneficial effects and enhances endogenous repair after SCI. This is the first study to demonstrate the efficacy of HGF for SCI.

Key words: hepatocyte growth factor; spinal cord injury; repair; functional recovery

Spinal cord injury (SCI) is followed by secondary degeneration, which is characterized by progressive tissue necrosis, and many experimental interventions using neurotrophic factors have focused on this posttraumatic inflammatory process to reduce damaged area and promote axonal regeneration throughout the lesion epicenter. Neurotrophins such as nerve growth factor (NGF; Tuszynski et al., 1994, 1996), brain-derived growth factor (BDNF; Jakeman et al., 1998; Vavrek et al., 2006), neurotrophin-3 (NT-3; Grill et al., 1997; McTigue et al., 1998), and glial cell line-derived neurotrophic factor (GDNF; Liu et al., 1999; Blesch and Tuszynski, 2001) have been reported to enhance axonal growth in injured spinal cord, and some of the studies cited above showed that neurotrophins promoted behavioral recovery after SCI (Jakeman et al., 1998; Liu et al., 1999).

Not only neurotrophic support but also angiogenesis after SCI is a critical factor in the endogenous regenerative response to trauma (Casella et al., 2002; Loy et al., 2002). Initial damage to local blood vessels is decisive for the progression of destructive events during secondary degeneration (Mautes et al., 2000) and strategic treatments to improve angiogenesis after SCI showed a relationship between blood flow and functional recovery (Glaser et al., 2004; Guizar-Sahagun et al., 2005). Hepatocyte growth

The first two authors contributed equally to this work.

Contract grant sponsor: Leading Project for the Realization of Regenerative Medicine from the Ministry of Education, Culture, Sports, Science and Technology (MEXT), Japan; Contract grant sponsor: General Insurance Association of Japan; Contract grant sponsor: Terumo Foundation Life Science Foundation (to H.O.); Contract grant sponsor: Grant-in-Aid for the 21st Century COE Program from MEXT (to Keio University); Contract grant sponsor: Keio Gijuku Academic Development Funds.

*Correspondence to: Hideyuki Okano, 35 Shinanomachi, Shinjuku-ku, Tokyo 160-8582, Japan. E-mail: hidokano@sc.itc.keio.ac.jp

Received 1 March 2007; Accepted 26 March 2007

Published online 4 June 2007 in Wiley InterScience (www.interscience.wiley.com). DOI: 10.1002/jnr.21372

factor (HGF) was first identified as a potent mitogen for mature hepatocytes (Nakamura et al., 1984; Nakamura et al., 1989) and a natural ligand for the c-Met protooncogene product (Bottaro et al., 1991). Recent studies have revealed that HGF acts as a neurotrophic factor in a variety type of neurons (Hamanoue et al., 1996; Maina and Klein, 1999; Caton et al., 2000) and that HGF administration enhances angiogenesis, improves microcirculation, inhibits the destruction of the blood–brain barrier (Date et al., 2004), and exerts a neurotroprotective effects after cereberal ischemia (Miyazawa et al., 1998; Shimamura et al., 2006). In the present study, we first examined the changes in endogenous HGF and c-Met expression after rat SCI and then determined whether the administration of exogenous HGF into the injured spinal cord using HSV-1 vector had positive effects on histological changes and the motor function after SCI. To the best of our knowledge, this is the first study to examine the efficacy of HGF for SCI.

MATERIALS AND METHODS

Administration of HGF by HSV-1 Vector and SCI

Adult female Sprague-Dawley rats (230–250 g; Clea, Tokyo, Japan) were used for all the experimental groups. All animals were handled in accordance with the Laboratory Animal Welfare Act, the *Guide for the care and use of laboratory animals* (National Institutes of Health), and the guidelines and policies for animal surgery provided by the Animal Study Committee of the Central Institute for Experimental Animals of Keio University. Rreplication-incompetent HSV-1 vectors, HSV-HGF and HSV-LacZ, were obtained as described by Zhao et al. (2006). Rats were anesthetized, their spinal cords were exposed by laminectomy at T10, and 10 μl of HSV-HGF or HSV-LacZ (each titer 1.3×10^9 pfu/ml) was injected into the spinal cord in the HGF group or the LacZ group, respectively (n = 62 each). At 3 days after HSV-1 vector injection, the spinal cords were again exposed at the site of injection, and the region was contused by using the Infinite Horizon impactor (200 kdyn; Precision Systems, Lexington, KY). In the SCI group, contusive SCI was induced at T10 using the IH impactor without the prior injection of HSV-1 vectors (n = 75).

Enzyme-Linked Immunosorbent Assay

Plasma samples were withdrawn transcardially, and a 4-mm-long segment of spinal cord at T10 was isolated and lysed at the indicated times. The spinal cord lysates were prepared with 50 mM Tris-HCl (pH 7.4), 2 M NaCl, 25 mM β-glycerophosphate, 25 mM NaF, 1% Triton X-100, 1 mM phenylmethylsulfonylfluoride (PMSF; Wako, Osaka, Japan), 2 mg/ml antipain (Peptide Institute Inc., Osaka, Japan), 2 mg/ml leupeptin (Peptide Institute Inc.), and 2 mg/ml pepstatin (Peptide Institute Inc.). The concentrations of HGF protein in the extracts of spinal cords lysates and plasma were determined by using ELISA kits (Institute of Immunology, Tokyo, Japan).

Real-Time Quantitative RT-PCR

A 4-mm-long spinal cord segment at T10 was collected at indicated times, and total RNA was isolated from each spinal cord sample using an RNeasy Kit (Qiagen, Bethesda, MD). The levels of HGF and c-Met mRNA were measured as previously described (Sun et al., 2000). The quantitative data for each sample at indicated times was used to determine the ratio relative to that in intact spinal cord.

Immunoblotting Analysis

Lysates from each 4-mm-long spinal cord at T10 were prepared in the same buffer used in an ELISA at indicated times. Proteins (20 μg) were resolved via SDS-PAGE, transferred to a polyvinylidene difluoride membrane, and immunoblotted with a polyclonal antibody (anticleaved caspase-3; 1:500; Cell Signaling Technology, Beverly, MA). Bands were visualized by using an ECL Blotting Analysis System (Amersham Bioscience, Arlington Heights, IL), and the band intensities were measured with an NIH image analyzer. The quantitative data for each band show the relative ratio to that of the spinal cord lysate at 3 days after SCI without any HSV-1 vector injection.

Immunohistochemistry

Spinal cords were perfusion fixed with 4% paraformaldehyde in 0.1 M phosphate-buffered saline (PBS) and postfixed in the same fixative (24 hr), 10% sucrose in 0.1 M PBS (24 hr), and 30% sucrose in 0.1 M PBS (24 hr). Segments of spinal cords were embedded in optimal cutting temperature compound and cut on a cryostat into 20-μm-thick sections. For immunofluoroscence staining, the sections were incubated at 4°C with monoclonal anti-NeuN (1:200; Chemicon, Temecula, CA), monoclonal antiglial fibrillary acidic protein (GFAP; 1:500; Sigma, St. Louis, MO), monoclonal anti-GST-π (1:500; BD Bioscience Pharmingen, San Diego, CA), and polyclonal anti-c-Met (1:50; Santa Cruz Biotechnology, Santa Cruz, CA), followed by Alexa Fluoro-conjugated secondary antibodies (1:500; Molecular Probes, Eugene, OR) and polyclonal anti-rat HGF (1:1; Institute of Immunology) and polyclonal anticleaved caspase-3 (1:400; Cell Signaling), followed by biotinylated secondary antibodies (1:500; Jackson Immunoresearch, West Groove, PA). For diaminobenzidine staining, the sections were incubated at 4°C with polyclonal anti-5-hydroxytryptamine (5-HT; 1:100; Dia Sorin, Stillwater, MN), polyclonal anticholine acetyltransferase (ChAT; 1:50; Chemicon), monoclonal anti-rat endothelial cell antigen-1 (RECA-1; 1:25; Serotec, Raleigh, NC), monoclonal anti-growth-associated protein-43 (GAP-43; 1:2,000; Chemicon), and monoclonal antineurofilament 200 kD (RT97; 1:2,000; Chemicon), followed by biotinylated secondary antibodies (1:500; Jackson Immunoresearch). Biotinylated antibodies were visualized using the Vectastain Elite ABC kit (Vector Laboratories, Burlingame, CA), followed by TSA (Vector Laboratories) or diaminobenzidine (Sigma). All the images were obtained via microscopy (Axioskop 2 Plus; Zeiss, Oberkochen, Germany) or confocal microscopy (LSM510; Zeiss).

Quantitative Analyses

To quantify the RECA-1-positive area and Luxol fast blue (LFB)-stained myelinated area, the images of axial sections were obtained. To quantify the area of the GAP-43-positive fibers and the RT97-positive fibers, the midsagittal sections were scanned and tiled transversely throughout a cephalocaudal

length of 175 μm at the indicated levels of injured spinal cords with a CCD camera (DXC-390; Sony, Tokyo, Japan) using a Micro Computer Imaging Device (MCID; Imaging Research Inc., St. Catharines, Ontario, Canada). The obtained images were analyzed using grain counting with the light intensity by MCID. Threshold values were maintained at constant levels for all analyses. Images of axial sections stained with hematoxylin and eosin were obtained, and manually outlined areas of cavitation were also quantified by MCID. Images of axial sections stained with anti-ChAT antibody and anti-RECA-1 antibody were obtained, and the numbers of ChAT-positive motoneurons in the ventral horns and the numbers of RECA-1-positive vessels with lumina larger than 20 μm were counted.

Behavioral Testing

Motor function of the hindlimbs was evaluated by open-field testing using the methodology of the Basso-Beattie-Bresnahan (BBB) scale at 4, 7, 14, 21, 28, 35, and 42 days after SCI (n = 14 for each group). Throughout the surgery, behavioral testing, and histological analyses, the three researchers who performed the procedures were unaware of the groups to which the rats belonged.

Statistical Analysis

All data are reported as the mean ± SEM. An unpaired two-tailed Student's *t*-test was used for single comparisons. The results of the real-time PCR and ELISA experiments were analyzed via Dunnett test. The Mann-Whitney U-test was used for the BBB score.

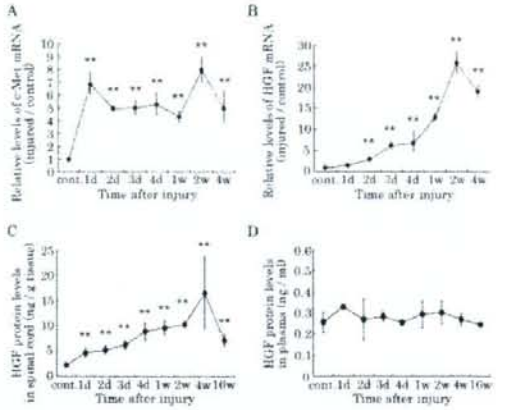

Fig. 1. Endogenous regulation of HGF and c-Met expression after SCI. The levels of c-Met mRNA and HGF mRNA expression after SCI in a 4-mm segment of spinal cord from the lesion epicenter were analyzed by using real-time RT-PCR. In contrast to a drastic increase in c-Met mRNA expression during the acute phase of SCI (**A**), HGF mRNA expression showed a gradual increase only during the subacute phase (**B**). ELISA data show that the amount of HGF protein in a 4-mm segment of spinal cord from the lesion epicenter gradually increased during the subacute phase of SCI (**C**), similar to the pattern of HGF mRNA expression, and the plasma HGF levels did not increase significantly after SCI (**D**). All data were reported as the mean ± SEM. $^{**}P < 0.01$; n > 3 each.

RESULTS

Endogenous Up-Regulation of HGF in Injured Spinal Cord Was Insufficient Compared With the Sharp Increase of c-Met Expression During the Acute Phase of SCI

To determine the dynamics of the HGF-c-Met system in adult rat spinal cord after SCI, the levels of HGF and c-Met mRNA expression in injured spinal cord were analyzed via real-time RT-PCR, and the amounts of HGF protein in injured spinal cord and plasma were also analyzed by an ELISA in the SCI group. Whereas the level of c-Met mRNA expression in injured spinal cord drastically increased from 1 day after SCI (Fig. 1A), the level of HGF mRNA expression gradually increased and peaked at 2 weeks after SCI (Fig. 1B). Thus HGF and c-Met mRNA expression peaked at different time points after SCI. Consistently with the level of HGF mRNA expression, the amount of HGF protein in injured spinal cord gradually increased, peaking at about 4 weeks after SCI (Fig. 1C). In contrast, the amount of HGF protein in the plasma did not increase after SCI (Fig. 1D). Next, we examined the localization of c-Met in normal and injured rat spinal cord. In intact thoracic spinal cord, c-Met immunoreactivity (c-Met-IR) was detected in NeuN-positive neurons and GST-π-positive oligodendrocytes, but not in astrocytes (Fig. 2A–I). However, at 1 week after SCI, c-Met-IR was clearly observed in GFAP-positive reactive astrocytes (Fig. 2J–L; axial section at 5 mm rostral to the epicenter) as well as in neurons and oligodendrocytes (data not shown).

To examine the distribution and amount of HGF protein in uninjured spinal cord after gene delivery, the spinal cord tissues were harvested and processed for an ELISA and HGF immunostaining at 3 days and 4 weeks after the HSV-1 vectors (HSV-HGF and HSV-LacZ) injection. Although HGF-IR showed a remarkable expansion putatively in the extracellular matrix in the HGF group at 3 days after injection, very little HGF-IR was observed in the LacZ group (Fig. 3A). Injection of the HSV-1 vectors resulted in a significantly higher amount of HGF protein in the HGF group (11.5 ± 0.8 ng/g tissue) compared with that in the LacZ group (3.4 ± 0.1 ng/g tissue) at 3 days after injection (Fig. 3C). Double immunostaining using anti-β-galactosidase antibody showed that LacZ gene expression was maintained in NeuN-positive neurons until 4 weeks after the injection (Fig. 3B). There was no significant difference in the amount of HGF protein between the HGF group (4.9 ± 1.5 ng/g tissue) and the LacZ group (2.9 ± 0.1 ng/g tissue) at 4 weeks after the injection (Fig. 3C).

HGF Promotes Survival of Neurons and Oligodendrocytes After SCI

To determine the effects of HGF gene delivery on the injured spinal cord, we performed several quantita-

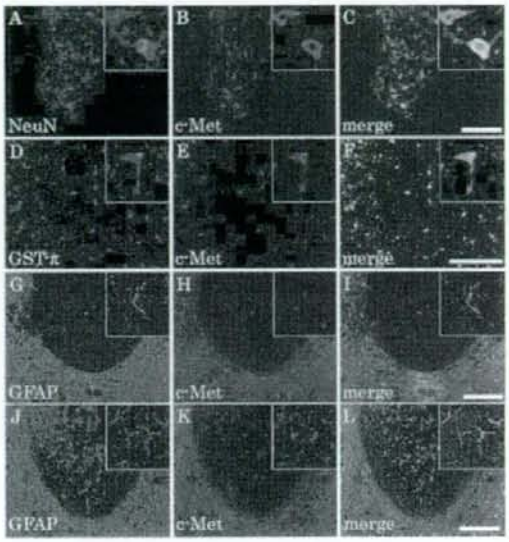

Fig. 2. Change in c-Met immunoreactivity (IR) in neurons, oligodendrocytes and astrocytes before and after SCI. Intact spinal cord showed c-Met-IR in NeuN-positive neurons (**A–C**) and GST-π-positive oligodendrocytes (**D–F**), but not in astrocytes (**G–I**). At 1 week after SCI, c-Met-IR was observed in GFAP-positive reactive astrocytes (**J–L**). **Insets** show magnified view. Scale bars = 200 μm in C (applies to A–C); 100 μm in F (applies to D–F); 200 μm in I (applies to G–I); 200 μm in L (applies to J–L).

tive histological analyses. First, the cavity area of the injured spinal cord at 6 weeks after SCI was obviously smaller in the HGF group than the LacZ group. Significant differences in the total cavity areas at the epicenter and at 4 mm rostral and caudal to the epicenter were observed between the two groups (Fig. 4A). Second, the HGF group obviously had more preserved myelinated areas than the LacZ group at 6 weeks after SCI. Notably, the HGF group exhibited a significantly spared rim of white matter, even at the lesion epicenter, whereas the LacZ group exhibited severely demyelinated white matter throughout the lesion epicenter. Quantitative analysis of the myelinated areas revealed significant differences between the two groups at all of the examined sites (Fig. 4B). Next, to determine the effect of HGF on motoneurons, the numbers of ChAT-positive motoneurons in the ventral horns were quantified at 6 weeks after SCI. Although almost all the ChAT-positive motoneurons had disappeared at the lesion epicenter in both groups, significantly larger numbers of ChAT-positive motoneurons were observed at the site rostral to the epicenter in the HGF group compared with that in the LacZ group (Fig. 4C). These findings suggested that HGF exerted protective effects on motoneurons and oligodendrocytes and contributed to tissue sparing after SCI.

Next, to determine whether HGF inhibited the activation of caspase-3 after SCI, immunoblotting analyses using anti-cleaved caspase-3 antibody were performed at 1, 3, and 7 days after SCI. Cleaved caspase-3 was strongly induced after SCI and was most detectable at 3 days after SCI in both the HGF and the LacZ groups (Fig. 5A). Quantitative analysis revealed that the induction of cleaved caspase-3 was significantly attenuated in the HGF group compared with the LacZ group at 3 days after SCI (Fig. 5B). Furthermore, double immunostaining with anti-cleaved caspase-3 antibody and antibodies for neurons or oligodendrocytes showed that the numbers of NeuN and cleaved caspase-3 double-positive motoneurons in the ventral horns and GST-π and cleaved caspase-3 double-positive oligodendrocytes were

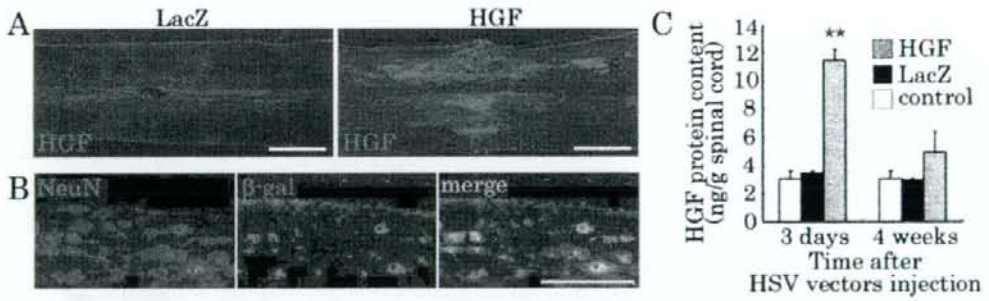

Fig. 3. Expression of exogenous HGF in the spinal cord introduced by HSV-HGF vector. Immunohistochemical staining of rat HGF in sagittal sections at 3 days after the HSV-1 vectors (HSV-HGF and HSV-LacZ) injection into the spinal cords showed remarkable HGF-IR in the extracellular matrix in the HGF group. In all the sagittal sections shown in the present study, the left side is the rostral side (**A**). β-Galactosidase expression was observed in neurons until 4 weeks after the HSV-LacZ injection (**B**). HGF protein levels in 4-mm segments of spinal cords at the site of the HSV-1 vectors injection were analyzed using an ELISA at 3 days and 4 weeks after the injection. The HGF group showed a significantly larger amount of HGF protein than in intact spinal cord (control) and the LacZ group at 3 days after injection. No significant difference in the amount of HGF protein was seen among the three groups at 4 weeks after the injection (**C**). $^{**}P < 0.01$; n = 3 each. Scale bars = 1 mm in A; 100 μm in B.

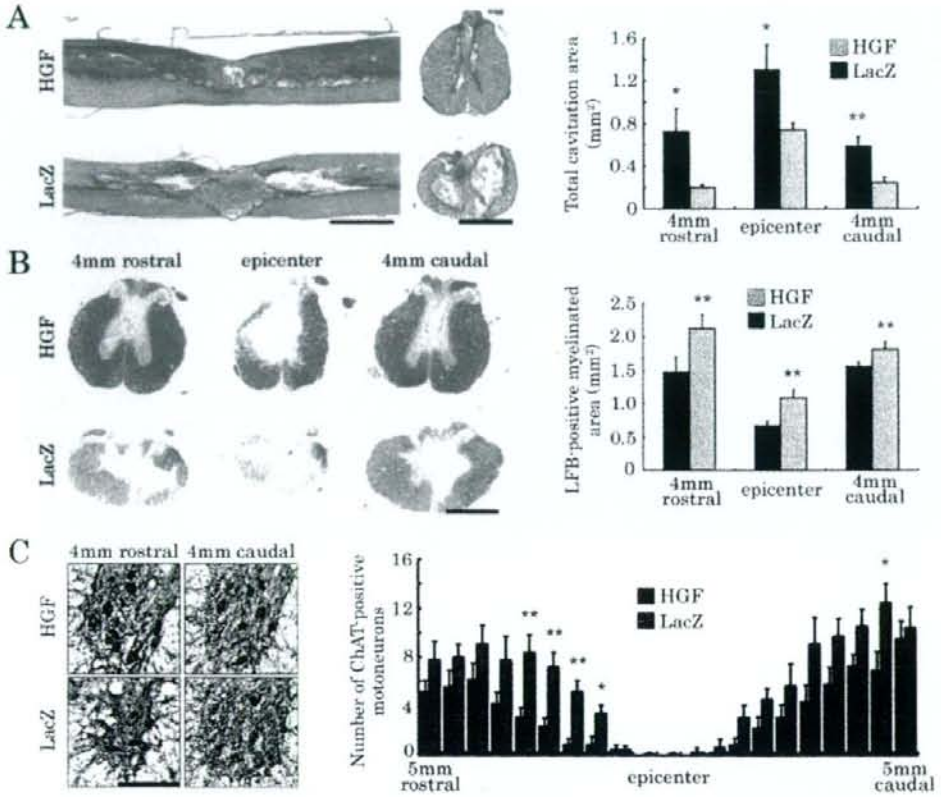

Fig. 4. Significant reduction in the size of damaged parenchyma in the HGF group. HE staining of midsagittal sections and the axial sections of lesion epicenter at 6 weeks after injury showed remarkably smaller areas of damage in the HGF group compared with the LacZ group. Significant differences in the total cavitation areas in the axial sections at the epicenter and at 4 mm rostral and caudal to the epicenter were observed between the two groups (n = 5 each; **A**). The axial sections stained with Luxol fast blue (LFB) at 6 weeks after injury showed a remarkable reduction in the area of demyelination in the HGF group compared with the LacZ group. Quantification of LFB-positive myelinated areas showed significant difference between the two groups at all of the examined sites (n = 5 each; **B**). The number of ChAT-positive motoneurons in the ventral horns at the lesion epicenter and adjacent sections up to 5 mm rostral and caudal to the epicenter in 0.5-mm increments was quantified at 6 weeks after SCI. The pictures show magnified views of right ventral horns of axial sections at 4 mm rostral and caudal to the epicenter. Significant differences between the two groups were observed mainly in the sections rostral to the epicenter (n = 5 each; **C**). $*P < 0.05$, $**P < 0.01$. Scale bars = 2 mm in A left; 1 mm in A right and B; 150 μm in C.

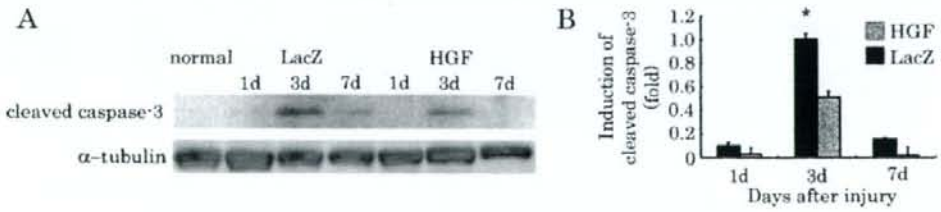

Fig. 5. Induction of cleaved caspase-3 in the injured spinal cord. Immunoblotting analyses showed remarkable induction of cleaved caspase-3 in the HGF and LacZ group during the acute phase of SCI, mainly at 3 days after SCI (**A**). Significantly attenuated cleaved caspase-3 induction was observed in the HGF group, compared with the LacZ group, at 3 days after SCI (n = 3 each; **B**). $*P < 0.05$.